Interactive metal mixture toxicity to *Daphnia magna* populations as an emergent property in a Dynamic Energy Budget Individual-Based Model

Simon Hansul[A], Andreas Fettweis[B], Erik Smolders[B], Karel De Schamphelaere[A]

[A]*Laboratory of Environmental Toxicology and Aquatic Ecology, Environmental Toxicology Unit (GhEnToxLab), Ghent University, Coupure Links 653 Building F - 2nd Floor, 9000 Ghent*, Belgium

[B]*Division of Soil and Water Management, KU Leuven, Kasteelpark Arenberg 20, 3001 Heverlee, Belgium*

Acknowledgement

We thank the Research Foundation of Flanders for financial support (project no. G046418). We thank Emmy Pequeur, Gisèle Bockstael, Jolien Depecker and Nancy de Sayer for technical assistance.

Data Accessibility statement

Data and code are available via Figshare. Code and usage instructions are additionally available via the GitHub profile of the lead author.

Interactive metal mixture toxicity to *Daphnia magna* populations as an emergent property in a Dynamic Energy Budget Individual-Based Model

Abstract

Environmental risk assessment of metal mixtures is challenging due to the large number of possible mixtures and interactions. Mixture toxicity data cannot realistically be generated for all relevant scenarios. Therefore, methods for prediction of mixture toxicity from single-metal toxicity data are needed.

We tested how well toxicity of Cu-Ni-Zn mixtures to *Daphnia magna* populations can be predicted with an Individual-based Model based on Dynamic Energy Budget Theory (DEB-IBM), assuming non-interactivity of metals on the physiological level.

We exposed *D. magna* populations to Cu, Ni, and Zn and their mixture at a fixed concentration ratio. We calibrated the DEB-IBM with single-metal data and generated blind predictions of mixture toxicity (population size over time), with account for uncertainty. We compared the predictive performance of the DEB-IBM with respect to mixture effects on population density and population growth rates with that of two reference models applied on the population level, Independent Action (IA) and Concentration Addition (CA).

Our inferred physiological Modes of Action (pMoA) differed from literature-reported pMoAs, raising the question whether this is a result of different model selection approaches, intraspecific variability, or whether different pMoAs might actually drive toxicity in a population context. Observed mixture effects were concentration and endpoint dependent. IA was overall more accurate than CA, but CA predicted effects on population growth rate

slightly better. The DEB-IBM most accurately predicted effects on 6-week density, including antagonistic effects at high concentrations, which emerged from non-interactivity at the physiological level.

Mixture effects on initial population growth rate appear to be more difficult to predict. To explain why model accuracy is endpoint-dependent, relationships between individual-level and population-level endpoints should be illuminated.

Keywords

Aquatic toxicology, metal toxicity, mixture toxicology, predictive toxicology, toxicity mechanisms, aquatic invertebrates, freshwater toxicology, computational toxicology

Introduction

Ecosystems might be at risk from contamination with mixtures of chemicals. When Environmental Risk Assessment (ERA) takes possible mixture effects into account at all, it relies on the application of relatively simple reference models. A major challenge is the sheer number of mixtures that might be relevant for risk assessment, and the possibility of synergistic and antagonistic effects. Since it is not feasible to test all mixtures of interest experimentally, it is necessary to develop models which allow to extrapolate from single-substance toxicity to mixture toxicity under untested conditions. In addition, environmental protection goals are usually formulated on the level of populations and higher, and therefore such models should allow to account for ecological processes and their interaction with mixture toxicity.

From individuals to populations

For various reasons, toxicity to populations can differ from toxicity to individuals. Firstly, population-level effects include the combined effects on lethal and sublethal individual-level endpoints. Secondly, in populations, individuals contribute to population-level effects during their entire lifecycle, and thus individual-level toxicity parameters which are specific for exposure duration, such as ECx-values, are of limited use to predict population-level responses. Thirdly, long-term individual-level toxicity tests are typically conducted without food limitation (OECD, 2012). In contrast, individuals in populations share an environment and thus food resources are limited. Limited food availability can result in altered toxicity to individuals (Heugens et al., 2006), but also lead to compensatory dynamics due to toxicant-

induced release from intraspecific competition, potentially leading to a lower sensitivity of population-level endpoints (Pereira et al., 2019). In addition to resource competition, physiological inhibition due to release of semiochemicals, or by physical interaction, can be relevant mechanisms of intraspecific interaction (Gergs et al., 2014).

Synergistic and antagonistic effects

When dealing with mixture effects, it is desirable to identify cases of synergistic or antagonistic effects. Stating that a mixture effect is synergistic or antagonistic is only meaningful if a reference model is defined (Cedergreen, 2014). Two reference models for mixture toxicity are widely established, being Independent Action (IA) and Concentration Addition (CA). Under the IA model, responses y_i, relative to a control, when exposed to a single substance i are combined multiplicatively to generate the predicted response to the mixture y_{IA} :

$$y_{IA} = \prod_{i=1}^{n} y_i$$

Equation 1

In order for equation 1 to generate meaningful predictions, y_i mu to be positive. For binary endpoints, this is treating the mixture response as the combined probability of n independent events. For discrete and continuous endpoints the mathematical application is identical.

CA-predicted responses result from the assumption that toxic units TU_{ECx} add up to one in a mixture giving x effect (Loewe & Muischnek, 1926):

$$\sum TU_{ECx} = \sum_{i=1}^{n} \frac{c_i}{ECx_i} = 1$$

Equation 2

c_i is the exposure concentration of substance i in the mixture and ECx_i is the concentration of i that elicits x percent of the maximum effect when *i* is tested individually.

Both reference models, by definition, assume non-interactivity of stressors. CA is generally expected to apply when stressors have similar Modes of Action and IA when stressors have dissimilar Modes of Action (Faust et al., 2003).

Deviations from reference models might depend on concentration ratios or levels (Jonker et al., 2005; Loureiro et al., 2010). For example, Nys et al. (2015) reported concentration-level dependent synergistic effects of nickel-zinc mixtures on *Daphnia magna* reproduction. Interaction with other ions in the test medium, or lack thereof, can also drive interactive mixture toxicity (Versieren et al., 2014).

Mechanistic effect modelling

With the addition of concentration level- and concentration ratio-dependent deviation factors (Jonker et al., 2005), static descriptions of mixture toxicity can be highly flexible. However, given that statistical models generally do not allow for extrapolation to untested conditions (e.g. different food levels or exposure durations), mechanistic effect modelling (Grimm & Martin, 2013) might be a more promising tool for predictive modelling of mixture toxicity.

To predict toxic effects under untested conditions mechanistically, Dynamic Energy Budget (DEB) Theory (Kooijman, 2010) is a useful framework. The core idea of DEB theory is that, as organisms take up energy, it is assimilated with a given efficiency and allocated to somatic growth, maintenance of structure, maturation and reproduction. A fixed fraction κ of assimilated energy is allocated to somatic growth and maintenance of structure, whereas the remaining fraction $1-\kappa$ is allocated to reproduction and maturity maintenance. A widely used extension of DEB theory is the implementation of sublethal effects of single metals or mixtures, in terms of effects on a selected physiological Mode of Action (pMoA), which represent a modification of one or more DEB parameters or energy fluxes (Jager et al., 2006). This approach has been applied to different taxa (Ashauer & Jager, 2018), but particular experience in this context has been gained with the standard test species *Daphnia magna*. Common applications include modelling of time-varying exposure to chemical stressors (Pieters et al., 2006) and analysis of toxicity based on multiple endpoints (Billoir et al., 2007; Jager et al., 2010). Pereira et al. (2019) used an Individual-based model based on DEB theory (DEB-IBM) to extrapolate nickel toxicity from individuals to populations at different temperatures, and correctly predicted the absence of effects on the population level when exposed to the median effective concentration for reproduction on the individual level. (Vlaeminck et al., 2021) applied the same approach to prediction of Copper-Zinc mixture toxicity to *D. magna* populations from individual-level single-metal toxicity.

Jager et al. (2010) proposed an approach to implement mixture toxicity in a DEB context, and demonstrated this using the toxicity of two polycyclic aromatic hydrocarbons to *D. magna*. If stressors have different pMoAs, implementation of mixture toxicity is relatively straightforward, since they can be applied independently (assuming that uptake and elimination processes occur independently). If the stressors have a shared pMoA, mixture toxicity might be implemented based on the assumption of different or shared molecular targets (given that a change in a particular physiological process, such as assimilation efficiency, might occur via different molecular targets (Jager et al., 2006)). We hereafter refer to the "different target" and "shared target" implementations as IA and CA on the physiological level, respectively. In the case study provided by Jager et al. (2010), model selection was done by fitting both models to mixture toxicity data and selecting the model that described the data best. This approach is suitable to identify mechanisms of mixture toxicity that are suggested by the model. However, if the aim is to perform blind predictions of mixture toxicity, one has to make assumptions on how mixture toxicity might be best represented on the physiological level. In the case of metals, this is further complicated by the fact that they do not have a single, identifiable molecular target. Therefore, making an *a priori* decision on whether metals should be considered as "different target" or "shared target" substances is not straightforward. While detailed knowledge on physiological mechanisms of metal toxicity to *D. magna* is available for some metals (Brix et al., 2017; De Schamphelaere & Janssen, 2002, 2004), this information is not easily converted to appropriate assumptions for mechanistic modelling of mixture effects. Nys et al. (2017) conducted a meta-analysis on the accuracy of IA and CA concerning metal mixture toxicity to three species, and concluded that IA is overall more accurate than CA. However, the involved studies mostly focus on individual-level toxicity, and it is therefore not clear whether the assumption of IA is also valid on the physiological level.

Uncertainty in mechanistic models

Individual-based Models (IBM) facilitate the use of mechanistic effect modelling with respect to ecological interactions (Martin et al., 2012; Pereira et al., 2019; Vlaeminck et al., 2021). Calibration of IBMs typically relies on numerical optimization algorithms, such as Approximate Bayesian Computation (ABC) (van der Vaart et al., 2015). When calibrating a model that includes mixture toxicity, a separate submodel has to be calibrated for each stressor in the

mixture. Consequently, when combining the results of those calibrations, their uncertainties are combined in the final model. It is unclear what the consequences of this combined uncertainty are concerning the accuracy and potential bias of IBM-predicted toxic effects. However, using the results of Bayesian optimization algorithms, it is possible to generate model predictions with account for uncertainty. Instead of using a point estimate to generate predictions, one might repeatedly sample values from the posterior distribution (van der Vaart et al., 2015), evaluate the IBM for each sample and thus map a distribution of parameter values to a distribution of predictions. The application of such an approach has been demonstrated before for toxicokinetic models (Ashauer et al., 2010), but not in combination with individual-based models or mixture toxicity.

Objective

In this study, we aimed to evaluate whether a DEB-IBM approach can be used to predict toxicity of Cu-Ni-Zn mixtures based on the assumption of IA on the physiological level, given constraints in the available data for model calibration, and using only single-metal toxicity data for calibration. We hypothesized that interactive mixture toxicity on the population-level can emerge from non-interactivity on the physiological level. More specifically, we assumed IA on the physiological level because it is the simplest to apply without estimating parameters from mixture data, and based on the existing evidence on individual-level mixture toxicity (Cedergreen, 2014; Nys, Versieren, et al., 2017). We conducted a microcosm population experiment with *D. magna,* exposing populations in a single-ray-design (Cedergreen et al., 2007) to Cu, Ni and Zn at environmentally realistic concentration ratios. We used data from the control and single-metal treatments to estimate DEB and toxicokinetic/toxicodynamic (TKTD) parameters and generated predicted mixture responses based on the assumption of non-interactivity on the physiological level and with account for uncertainty in parameter estimation. We first analyzed observed mixture responses statistically, to establish whether the data provides evidence for interactive mixture effects.

We then compared DEB-IBM-predicted with observed responses in the mixture treatments, to evaluate the accuracy of blind predictions relative to the accuracy of reference mixture models.

Materials and Methods

Population Experiment

We obtained a clone of *D. magna* from the Laboratory of Aquatic Ecology, Evolution and Conservation, KU Leuven. The clone was originally sampled from Langerodevijver, Belgium (50.828581N, 4.639960E), and was cultured for 3 months in our laboratory before onset of the experiments.

Organisms were cultured in a COMBO (Kilham et al., 1998) medium, modified to represent more environmentally relevant conditions (55 mg $CaCl_2 \bullet 2H_2O$ L^{-1}, 55 mg $MgSO_4 \bullet 7H_2O$ L^{-1}, 1 mg H_3BO_3 L^{-1}) and without the addition of N or P. The cultures were kept in a climate controlled room at 20°C and a 16:8 Light-Dark cycle. pH of the medium was adjusted to 7.5 (±0.2) by adding HCl to a final concentration of 0.5 mM. No further pH buffers were used. Culture media were aerated and allowed to equilibrate for at least 24h before use.

Test media and conditions were identical to the cultures except for the addition of natural DOC (4 mg L^{-1}) to test media instead of EDTA. Natural DOC had been sampled by reverse osmosis in November 2018 from the Schwarzbach stream (East-Belgium, 50.5210522N, 6.205860E), fractionated by acidification, de-ionized via H^+-cation exchange and freeze-dried (De Schamphelaere et al., 2003). The freeze-dried material was dissolved in 15 mM NaOH and added to the test medium as combined Fe+DOC stock. 10 mL Fe+DOC L^{-1} were added to reach a $FeCl_3 \bullet 6H_20$ concentration of 0.77 mg L^{-1} in the medium. Reverse osmosis had previously been shown to not affect protectiveness of DOC with respect to Cu and Zn toxicity (De Schamphelaere et al., 2005) . Metal-spiked test media were allowed to equilibrate for at least 48h before use.

We initiated populations with 2 egg-carrying females (age 7 to 21 days) and 8 neonates (<=24h) in 500 mL medium contained in a 1000 mL polypropylene jar (Avamoplast, Lokeren, Belgium). Populations were daily fed a diluted mixture of *Raphidocelis subcapitata* (also known as *Pseudokirchneriella subcapitata*) and *Chlamydomonas reinhardtii* in a 3:1 cell-based ratio, totaling 8×10^7 cells L^{-1}, corresponding to approximately 2.5 mgC L^{-1}.

Twice per week, we percolated test media over a 200 µm sieve, retaining all *D. magna* individuals. We transferred populations from the sieve to a petri dish with fresh test medium, where we determined population sizes by taking a series of images with a digital camera

(EOS200D, Canon, Tokyo, Japan), connected to a laptop computer and controlled by an xml script, and counting animals from the images using the Cell Counter plugin in ImageJ 1.52j. Because we took a series of images from identical positions at identical time-intervals, we could identify immobilized individuals, which were not counted. We then re-combined populations and fresh medium with old medium to reach 25% renewal.

Once per week, we took two integrated 10 mL samples of new and old media per treatment. Both were passed through a 0.45 µm filter (Acrodisc, Pall Life Sciences). One was acidified with HNO_3 to a final concentration of 0.14 M and used for analysis of metal concentrations and major cations (ICP-OES). Details on ICP-OES measurements are given in Supporting Information (SI Table 1-3). The other sample was used for analysis of DOC concentrations (TOC-L, Shimadzu, Kyōto, Japan). At the same occasions, pH was measured using a pH electrode (p407, Consort, Belgium) in old and new media.

We exposed populations to a control, Cu, Ni and Zn and their tertiary mixture with five concentrations per exposure type and four replicates per treatment combination. Nominal metal concentrations were arranged in a geometric series with a fixed, environmentally relevant mass ratio of 1:1:3 Cu:Ni:Zn (Van Regenmortel et al., 2017), ranging from 5 to 250 µg Cu and Ni L^{-1} and 15 to 750 µg Zn L^{-1}.

Speciation and exposure modelling

We converted measured metal concentrations to free ion activities with WHAM VII (Tipping et al., 2011), based on measured pH, DOC, dissolved Na, Mg, K, Ca, Ni, Cu, and Zn and nominal total Cl, SO_4 and CO_3. For specific assumptions, see (Nys, Janssen, et al., 2017). As solute database, we used the updated National Institute of Standard and Technology (NIST) database (Smith et al., 2004). All constants reported in the NIST database were included. As input for model simulations, we used a continuous time-series derived from the WHAM VII-predicted free ion activities. Measured concentrations, however were only available on a weekly basis. To deal with this, we performed a step-interpolation between measurements. The details of these calculations are described in Supporting Information.

The time-series of free-ion activities predicted by WHAM for each treatment are shown in SI Figure 3 and SI Figure 4.

Individual-based Model

All data treatment and modelling except for speciation modelling was done in Julia 1.3.0. A schematic overview of the modelling scheme is given in SI Figure 1.

Our DEB-IBM implementation was derived from Pereira et al. (2019), which had in turn been derived from the generic DEB-IBM implementation by Martin et al. (2012). The toxicity submodel was a combination of the reduced General Unified Threshold Model of Survival (GUTS-RED, Jager et al., 2011) and the DEBtox approach (Jager et al., 2006). A major difference between our DEB-IBM implementation and previous implementations was that, *a priori*, we allowed for stressors to act via arbitrary combinations of pMoAs. We decided to do so in order to be able to explain some of the more complex single-metal responses, and because different combinations of pMoAs might have different implications for mixture toxicity on the population-level. In addition to the assumptions that are inherent to DEB, DEBtox and GUTS, we made three additional major assumptions:

Firstly, the model included a single food source. In the population experiment, populations were fed a mixture of two algal species. We did not model those explicitly, but modelled food dynamics as if there was only one type of resource, using total food density (# cells L^{-1}) as input variable. We think this simplification is justified because the composition of the added food mixture was constant throughout the experiment, and because daphnids are, under most circumstances, unselective filter feeders (Lampert, 1974), so it is to be expected that the estimated parameters represent the modelled system equally well across treatments and time-points. Secondly, we assumed non-interactivity of metals at the physiological level: In reality, metals might mutually affect their uptake and elimination or binding to target sites, and thus interact on a molecular or cellular level. In the model, we assumed metal toxicokinetics and toxicodynamics to be independent. Combined effects on shared pMoAs were applied by assuming IA on the physiological level. Thirdly, we assumed one damage pool per metal: We modelled toxicity with one damage pool per metal, rather than a separate damage pool for every pMoA, thereby avoiding the estimation of a separate k_d value for every pMoA. This means that each metal can have multiple toxicodynamic components, but only one toxicokinetic component.

Following GUTS-RED, external concentrations $C_{W,i}$ (nM Me^{2+}) of metal i were directly translated to scaled damage $D_{W,i}$, (nM Me^{2+}) controlled by a single parameter, the dominant rate constant k_d (day^{-1}):

$$\frac{dD_{W,i}}{dt} = k_{d,i} \times (C_{W,i} - D_{W,i})$$

Equation 3

Sublethal and lethal effects were modelled as a function of a common damage pool $D_{W,i}$ for each metal.

In the case of lethal effects, we related $D_{W,i}$ to a hazard rate $h_{z,i}$ (day^{-1}) using a log-logistic equation, and converted $h_{z,i}$ to a stochastic mortality probability $p_{z,i}$.

$$h_{z,i} = \frac{h_{max,i}}{1 + \left(\frac{D_{W,i}}{ED50_{h,i}}\right)^{-\beta_{h,i}}}$$

Equation 4.1

$$p_{z,i} = \mathrm{e}^{-\mathrm{h_{z,i}}}$$

Equation 4.2

We thus assumed a stochastic death mechanism. In Equation 4.1, we deviate from the original GUTS formulation, where a hockey-stick equation with a threshold concentration and a slope is used to relate damage to hazard rate. The mortality probability $p_{z,i}$ was evaluated independently for each metal. $ED50_{h,i}$ (nM) is the scaled internal damage that leads to 50% of the maximum hazard rate caused by stressor i, $h_{max,i}$; $\beta_{h,i}$is the corresponding Hill's slope.

For implementation of sublethal effects, we related $D_{W,i}$ to physiological stress S_i specific for pMoA j:

$$S_{i,j} = \frac{S_{max,i,j}}{1 + \left(\frac{D_{W,i}}{ED50_{S,i,j}}\right)^{-\beta_{S,i,j}}}$$

Equation 5

$ED50_{S,i,j}$ is the 50% effective damage of metal i with respect to pMoA j. $S_{max,i,j}$ $(-)$ is the corresponding maximum stress level. The state variable $S_{i,j}$ modifies physiological processes based on the physiological Mode of Action (pMoA). We considered the four most commonly considered pMoAs (Jager et al. , 2010), being 1), increase in growth costs, 2) increase in somatic and maturity maintenance costs, 3) decrease in assimilation flux, 4) decrease in reproduction efficiency (SI Table 4).

In addition, we fitted a mortality constant m_e which results in increased mortality at reduced scaled reserve density (Martin et al., 2013) and generally dampens oscillatory fluctuations of population density over time. In DEB, the scaled reserve density e (-) is the amount of reserve relative to the maximum amount of reserve, or reserve capacity. It can take values between 0 and 1 and converges to one if an individual's assimilation rate is at its maximum. Based on m_e and e, a mortality probability p_e is calculated at every time-step of the model.

$$p_e = (1 - e)(m_e)^{\frac{1}{TR}}$$

Equation 6

TR (# time-steps day^{-1}) is the temporal resolution at which the IBM is executed.

For further model analysis, we investigated predicted population-averages of some DEB-IBM state variables, namely the scaled ingestion rate $\dot{J_X}$ (# cells day^{-1}), functional response f (-),and assimilation rate $\dot{p}$ $(J\ day^{-1})$ (see Supporting Information for more details).

A model description according to the Overview, Design Concepts and Details (ODD) protocol (Grimm et al., 2010) is given in Supporting Information.

Calibration

For parameter inference, we used a Sequential Monte Carlo Approximate Bayesian Computation (SMC-ABC) scheme, adapted from previously described algorithms (Sisson et al., 2007; Toni et al., 2009). Details about SMC-ABC are given in supporting information. Prior distributions were initially defined as Log-Normal distributions to conservatively cover the range of biologically plausible values, with standard deviations covering at least one order of magnitude. In some cases, Log-Normal distributions were replaced by narrower Uniform distributions to improve convergence behavior.

DEB parameters were fitted to population density in the control, using values from the Add-my-pet database (Kooijman & Gergs, 2019) as default. TKTD parameters were fitted to $\ln(y+1)$-transformed control-normalized densities over time. Because SMC-ABC is particle-based, covariance between parameters was accounted for.

Our model implementation allowed for simultaneous effects via five toxicity components (four pMoAs and direct lethal effects). This means that the SMC-ABC algorithm could converge towards a model where a single pMoA, or any combination of pMoAs drives metal toxicity. After parameter inference, we conducted additional Monte Carlo simulations to evaluate to which extent each component drives toxic effects in the calibrated models. This was done by simulating the single-metal treatments with each component acting separately (detailed scheme given in Supporting Information).

Mixture analysis

We analyzed deviations of observed responses from IA and CA predictions based on two endpoints, initial growth rate r (day^{-1}) and 6-week density (# Daphnids L^{-1}). Because observed population trajectories did not always fit a logistic growth curve, we calculated r based on the peak density N_{peak}, the initial density N_0 and the time to reach N_{peak}, t_{peak} (days).

$$r = \frac{\ln\left(N_{peak}\right) - \ln\left(N_0\right)}{t_{peak} - t_0}$$

Equation 7

If population density declines monotonically throughout the experiment, the denominator of this equation is 0 and r is not defined. We set r to 0 in these cases, despite the fact that a monotonically decreasing population has in fact a negative growth rate. The reasons for this decision were that firstly, any extinctions that occurred in the population experiment occurred within the first 7 days of exposure, and therefore differentiating between extinctions occurring at different paces (i.e., different negative values of r), was not of particular interest for our analysis. Secondly, negative responses would complicate the generation of IA-predicted responses, since multiplication with negative values is likely to lead to erroneous predictions, while at the same time not providing any additional insight in this particular case.

The IBM-predicted population growth rates were derived from the predicted time-series data the same way that population growth rates were derived from observed time-series data.

For 6-week density, we used the average population density in the last week of the experiment, to make this endpoint less prone to stochastic fluctuations in population density.

IA- and CA-predictions were generated based on relative responses, i.e. population density in a given treatment and at a given time-point divided by the control average at the same time-point. To generate IA-predicted responses y_{IA}, we multiplied observed relative responses of the corresponding endpoint to single metals. To generate CA-predicted responses over time, we treated subsets of the data as independent datasets, each subset consisting of the control-normalized population densities in all single-metal treatments at a given time-point. For each metal i at every time-point t in the single-metal tests, we performed nonlinear least squares regression (function *curve_fit* from the LsqFit package in Julia) on the observed relative responses versus WHAM-predicted free-ion activities in the single-metal treatments, to estimate a median effective concentration $EC50_{t,i}$ (nM) and Hill's slope $\beta_{t,i}$ (-) according to the following equation:

$$y_{t,i} = \frac{1}{1 + \left(\frac{C_{t,i}}{EC50_{t,i}}\right)^{\beta_{t,i}}}$$

Equation 8

$C_{t,i}$ is the WHAM-predicted free ion activity of metal i at time-point t. Since the effective concentration ECx is inversely related to the concentration-response function at response x, the CA-predicted response y_{CA} at time-point t was then determined by solving

$$\sum_{i=1}^{n} \frac{C_{t,i}}{EC50_{t,i} \times \left(\frac{y_{CA,tt}}{1 - y_{CA,t}}\right)^{\frac{1}{\beta_{i,t}}}} = 1$$

Equation 9

numerically (Nys et al., 2017), using SMC-ABC. n is the number of metals in the mixture.

To generate CA-predicted responses of growth rate and 6-week density, we fitted log-logistic curves to the single-metal responses and solved Equation 9 correspondingly.

To quantify deviations from reference models, we estimated the deviation parameter a for IA and CA (Jonker et al., 2005) with SMC-ABC, by solving equations 9.1 and 9.2 for CA and IA, respectively.

$$\sum_{i=1}^{n} \frac{c_{t,i}}{ECx_{t,i}} = \exp(G)$$

Equation 10.1

$$y_{IA} = \phi\left(\phi^{-1}\left(\prod_{i=1}^{n} y_{t,i}\right) + G\right)$$

Equation 10.2

ϕ is the cumulative distribution function of the standard normal distribution and G is the deviation function, which depends on the relative contributions to toxicity $z_i = \frac{TU_i}{\sum TU}$ and the deviation parameter a:

$$G = a \times \prod_{i=1}^{n} z_i$$

Equation 11

We tested for significant interactions using a nested F-test (Hochmuth et al., 2014). To account for multiple testing, we applied a Bonferroni correction. Given an initial significance level of 0.05 and 20 signficance tests conducted, this resulted in a significance level of $\alpha = \frac{0.05}{20} = 0.0025$.

Validation

Since there was only one measured variable available, but a total of 16 parameters to estimate for each metal, we expected our estimation of TKTD parameters to be associated with large epistemic uncertainty. To account for this, we refrained from deriving point estimates of parameters from posterior distributions. Instead, we generated predictions by running Monte Carlo simulations and sampling a particle from the posterior distribution in each step. This results in a distribution of predictions for each predicted data point, which maps the uncertainty in parameter estimation to the uncertainty in model output.

To generate predictions from the DEB-IBM, we sampled 100 independent particles from each of the four joint posterior distributions (one for DEB parameters and one for each metal) and simulated the experiment for each sample. The predicted growth rates and 6-week density were calculated for each sample separately.

Results

Physicochemistry

Mean measured physicochemical test media characteristics in the population experiment are reported in Table 1. In the first week of the experiment pH increased up to 9.9, likely due to photosynthetic activity of the added algae, but fell back down when *D. magna* population sizes increased (SI Figure 2).

Across all treatments (single-metals and mixture), mean measured dissolved metal concentrations deviated at most by a factor of 1.8 from nominal concentrations. The average ratio between mean measured and nominal concentrations across all treatments was 0.99 (SD=0.3, N=20). Mean measured metal concentrations in the mixture treatments deviated at most by a factor of 1.9 from measured concentrations in the corresponding single-metal treatments. Metal concentrations in the mixture treatments deviated from the corresponding single-metal treatments by an average factor of 1.08 (SD=0.28, N=15) (see SI Table 5 for all metal concentrations per treatment).

Average Cu concentration in the controls was 5.8 µg L^{-1}, which could potentially have contributed somewhat to background toxicity in *D. magna*. However, we have not observed adverse effects of Cu on initial growth rate or 6-week density at measured concentrations up to 13.4 Cu µg L^{-1} , suggesting that background toxicity of Cu was not an issue for the endpoints of interest. Without individual-level data, it cannot be ruled out entirely that some individual-level background toxicity occurred, which might have been compensated for on the population level. However, given the mean measured media physicochemistry (Table 1), the average bioavailable Cu concentration in the control was only 0.14 µg L^{-1}, and the bioavailability-corrected HC5 equal to 38 µg L^{-1} (both calculated in BIO-MET bioavailability tool Version 5-June 2019), which is 7 times above the average Cu concentration in the control.

Calibration

Population dynamics in the control followed a delayed logistic growth pattern, with a peak density of 877 (SD=55, N=4) daphnids L^{-1} at day 18, corresponding to an initial population growth rate of 0.21 day^{-1}. The mean final population density was 447 (SD=15.1, N=4) daphnids L^{-1}. We could approximate this pattern with the DEB-IBM by correcting food-dependent parameters (Table 2, Figure 1). Estimated values for parameters which are also reported in the add-my-pet database were within the range of values reported for different species of the genus *Daphnia*.

The DEB-IBM could be fitted well to single-metal control-normalized population densities. Only at the highest Ni concentration, the relative responses were continuously under-estimated (Figure 2). At intermediate concentration levels, we often observed effects on the initial exponential growth phase of the population, followed by partial or full recovery. A notably complex response pattern was observed at the second-highest Zn treatment (717 nM), where an effect on the exponential growth phase was followed by recovery of the population, which was in turn followed by collapse of the population. This was qualitatively and quantitatively reproduced by the DEB-IBM. Predicted responses were also adequate for initial growth rate and 6-week density (Figure 3). Notably, Ni did not affect population growth rates.

Posterior distributions of the estimated TKTD parameters were relatively broad (SI Figure 5-7, SI Table 6-8), but the variability in corresponding predicted responses was acceptable (the normalized root mean square error between fitted and observed values was below 0.1 in all cases), indicating that different parameter combinations predicted similar patterns.

Analysis of pMoAs suggested effects on reproduction efficiency as the main driver of toxicity for all three metals. For Zn, effects on assimilation flux contributed to toxicity at higher concentrations. Direct lethal effects played a subordinate role expect at the highest tested concentrations, where they contributed clearly to population extinction due to Cu and Zn (Figure 4). At the highest Zn concentrations, the observed population extinction was predicted to be caused by a combination of all pMoAs. However, since all populations went extinct within less than a week in these treatments, these subsets of the data do not provide much information on mechanisms of toxicity, and therefore we do not consider the combined

effects of pMoAs at high concentrations to be biologically relevant, since direct lethal effects alone might explain this pattern equally well.

Statistical analysis of mixture effects

Significance testing indicated statistically significant ($p<0.0025$) mixture interactions in all but the highest mixture treatments (Table 3). However, the high statistical significance was in many cases attributable to either a relatively low variability of observed responses, or to the fact that mixture models were fitted to every mixture treatment individually, due to the apparently high concentration-level dependency of deviations. Since the nested F-test is based on the Sum of Squared Errors of the fitted model and the null model, there is a high chance that even a small improvement of model fit compared to the null model leads to high statistical significance with this approach. Therefore, high statistical significance does not necessarily indicate toxicological concern.

The clearest interaction was found in the third-highest mixture treatment (Mix3, 29.7 µg Cu L^{-1}, 34.2 µg Ni L^{-1}, 90.1 µg Zn L^{-1}, $\sum TU_{EC50,r} = 0.56, \sum TU_{EC50,K} = 1.21$), where effects on growth rate as well as 6-week density were antagonistic. At the second-highest test concentration Mix4 (54.3 µg Cu L^{-1}, 68.9 µg Ni L^{-1}, 202 µg Zn L^{-1}, $\sum TU_{EC50,r} = 1.7$), effects on growth rate were on average synergistic relative to IA and antagonistic relative to CA (Figure 5).

Validation

Overall, the predictive performance of IA, CA and the DEB-IBM was comparable, though relative performance of the three models was highly endpoint- and concentration level-dependent, both in terms of responses of initial growth rate and 6-week density (Figure 5) as well as in terms of responses of population density over time (Figure 6). In the lowest mixture treatment ($\sum TU_{EC50,t} = 0.2$), observed responses over time matched IA- and DEB-IBM-predicted responses. In two mixture treatments ($\sum TU_{EC50,t} = 0.4$, $\sum TU_{EC50,t} = 2.8$,), observed responses were lower than IA predictions. This interactive effect was only predicted by the DEB-IBM for the higher treatment. At $\sum TU_{EC50,t}$=1.1, recovery of the population was observed, which was qualitatively predicted by the DEB-IBM, but delayed in time. Overall, the response over time showed concentration-level dependent deviations from reference models. In the highest mixture treatment ($\sum TU_{EC50,t}$=12.5), predicting extinction was trivial, since this was already fully explained by single-metal responses to Cu and Zn.

Expressed in responses of growth rate and 6-week density, the predictions of mixture effects to 6-week density were substantially more accurate than predictions of effects on growth rate (Table 4). The mixture dose-response of growth rate was not well predicted by any of the models, but slightly better by CA than IA and the DEB-IBM. Notably, the DEB-IBM over-estimated effects on growth rate at low concentrations, where mixture exposure was even observed to be associated with a slight stimulation of growth rates. The synergistic effect on growth rate in the second-highest mixture treatment was only partially predicted. Effects on 6-week density were best predicted by the DEB-IBM, including antagonistic effects at high concentrations (Figure 5).

According to the DEB-IBM predictions, exposure to single metals and mixtures was associated with stimulation of average ingestion rates (SI Figure 8-9), with similar effects on assimilation rates under Cu and Ni exposure (SI Figure 10). Under Zn exposure, average assimilation rates were also increased, but to a lesser extent than ingestion rates, due to the direct effect of Zinc on assimilation flux. In the mixture treatments, parts of the stimulating effect on average assimilation rates caused by Cu and Ni appeared to be mitigated by the effect of Zn, suggesting that interactions between pMoAs induce interactive mixture toxicity. More detailed information on predicted individual-level state variables is given in Supporting Information.

Discussion

Calibration

Calibration of a DEB-IBM with population-level data is possible, even if only population densities over time are available, which is traditionally not considered to be ideal to estimate DEB and TKTD parameters (Kooijman et al., 2008; Kooijman & Bedaux, 1996). We acknowledge that population density alone is insufficient to derive parameters that define uptake of food, assimilation and allocation of energy within organisms without uncertainty. To a lesser degree, this is also the case when parameters are estimated from life-table data, as typically generated in the course of ecotoxicological experiments with *Daphnia* (Kooijman et al., 2008). Uncertainty in parameter estimates is to some extent inherent to DEB-based models, since some of the parameters are unmeasurable or only measurable with immense experimental expenditure, and thus can only be estimated with uncertainty. We thus advocate the use of methods that propagate uncertainty when applying DEB-IBMs and similarly abstract models,

for example by running Monte Carlo simulations rather than using point estimates of parameters.

Adding to the advantage of the DEB-IBM approach, TKTD parameters are independent of exposure duration. Applying empirical mixture models requires ECx values which do depend on exposure duration (Jager, 2011), so concentration-response curves have to be fitted to every time-point of interest, which is not always a simple task, for example if concentration-response curves are not well described by a simple log-logistic function.

Physiological Modes of Action

Analysis of pMoAs indicated that effects on reproduction efficiency at individual level were a main driver of effects at population level for all three metals. This might be a consequence of the fact that the only available measurement was population density (# daphnids L^{-1}). In the given units, this is most directly reflected by varying reproductive output, rather than growth or maintenance rates. In other words, an effect on reproduction efficiency directly affects the number of individuals in the population, whereas an effect via other pMoAs first affects energy fluxes in other parts of the model, and only indirectly affects the number of individuals in the population, and therefore, the kind of measurement that is available might affect which conclusions about pMoAs are drawn. Therefore, the generalizability of the predicted pMoAs can be questioned. However, in the case of Zn, effects on assimilation rate were also essential for predicting the single-metal effects in addition to effects on reproduction efficiency, indicating that physiological processes other than reproduction were also accounted for. Our identified pMoAs were not in agreement with those reported in previous studies on *D. magna*. However, those amount to a relatively small number of studies (Cu and Zn: cf. (Ashauer & Jager, 2018; Vlaeminck et al., 2021), Ni: (Pereira et al., 2019)), and also used different approaches for parameter estimation. A hypothesis that might explain this deviation, and which has not been considered so far, is that pMoAs might be different in a population context than in an individual context, for example due to physiological adaptation of animals under long-term exposure, or mediated by crowding. If this is the case, extrapolation of toxicity across levels of biological organization might be limited with currently advocated approaches, and therefore this hypothesis deserves further investigation.

The approach we used for selection of pMoAs, i.e. to allow for arbitrary combinations of pMoAs, is not common in DEB-based modelling. A disadvantage of this approach is that a

larger number of parameters has to be estimated simultaneously. We think that the approach is nevertheless justified from different perspectives: from a practical point of view, an advantage of this approach is that only a single calibration per metal has to be run, and the final posterior distribution encompasses all models that describe the data to some degree. The influence and probability of different pMoAs can be analyzed *a posteriori*, but there is no need to decide for a single pMoA and exclude all other possibilities *a priori*. Furthermore, effects of Zn were in our case clearly best described by a combination of two pMoAs. At the same time, we have seen that if a single pMoA sufficiently explains the data, the SMC-ABC algorithm will converge toward that model, as was the case for Cu and Ni. I.e., the model will not necessarily be over-fitted, as one might expect if the potential model complexity is high. In addition, a more detailed model analysis (SI Figure 8, SI Figure 9) suggested that the interplay between simultaneously acting pMoAs was important for the prediction of interactive mixture effects.

It has to be noted that, given the ratio between estimated parameters and data-points in this calibration exercise, there is considerable uncertainty around the TKTD parameter estimates, as well as around the identification of pMoAs, and therefore the application of such a model should go hand-in-hand with uncertainty propagation techniques. As stated before, this uncertainty should caution against generalization of the pMoAs identified in this study to other model applications. We therefore present this modelling approach as proof of principle, showing the capacity of the DEB-IBM approach to predict mixture effects under limited data availability when combined with uncertainty propagation.

Predicting mixture effects to population-level endpoints

Based on the assumption of non-interactivity of metals on the physiological level, we could successfully apply the DEB-IBM approach to perform blind predictions of metal mixture toxicity to population-level endpoints, including correct predictions of antagonistic effects that resulted from the assumption of non-interactivity on the physiological level.

Predictions of mixture effects on 6-week density were substantially more accurate and more precise than those of effects on population growth rate. This discrepancy might be attributed to two inherent differences between these endpoints:

Firstly, 6-week density is an ergodic property of the system, i.e. does not change as a function of initial conditions when food and toxicant levels are kept constant. Rate of increase, on the other hand, is sensitive to initial conditions. Consequently, predictions of the rate of increase can more easily suffer from inaccuracies in the definition of initial conditions in the DEB-IBM. More precisely, our initial populations contained adult females, and thus the life-history of those individuals, prior to the onset of the experiment, has to be taken into account in the simulations. While we attempted to do so by predicting individual state variables of adult females under culture conditions, we did not have information on some crucial aspects such as the average number of eggs in the brood pouch at day zero. If growth rates are of interest, we therefore suggest to initiate populations with juveniles only, possibly of varying age to minimize fluctuations in population density due to synchronized reproduction. Alternatively, additional data about the life-history of initial adults may be recorded, in order to ensure that those are translated to the corresponding state variables of initial adults in the simulation.

Secondly, the calculation of rate of increase is always influenced by data-points with low population densities. These are subject to higher stochasticity and therefore, growth rates can be expected to be associated with higher variability than 6-week density and thus be harder to predict.

Taking these factors into account, however, it is still unclear why the DEB-IBM over-estimated effects on growth rate at low concentrations, and was unable to predict synergistic effects at high concentrations. We think that relationships between individual-level parameters and (mixture) effects on growth rate first have to be further clarified to explain this trend.

Analysis of predicted ingestion rates, assimilation rates and fecundity indicated that overall, compensation effects due to mitigation of food competition played an important role for (mixture) toxicity on the population-level. This also explains why for growth rate and 6-week density, different patterns of mixture toxicity can emerge: By the time that the population reaches steady state, food is always limiting, and therefore food limitation has a large influence on effects on 6-week density. In contrast, the initial growth rate encapsulates the time-window of the experiment where food is not limiting, or only starts to become limiting. Consequently, interactions between food competition and effects on growth rate vs effects on 6-week density should also be expected to be different.

Assuming non-interactivity of metals

The DEB-IBM predicted antagonistic effects on 6-week density relative to IA, despite IA being assumed on the physiological level. This predicted antagonism was in line with observed effects, which shows that interactive effects do not have to be implemented on the physiological level in order to explain interactive mixture effects on higher levels of organization. Analysis of individual-level state variables suggested that the predicted antagonistic effect was a result of the combined effects of metals via different pMoAs, namely reproduction efficiency and assimilation rate.

Our results indicate that the assumption of non-interactivity on the physiological level can be used in order to predict population-level metal mixture effects. However, a synergistic effect on growth rate was only partially predicted. Failure of the DEB-IBM to predict synergistic effects could point at interactive mixture toxicity on the individual level, which might be more important with respect to effects to population growth rate, compared to 6-week population density, given that population growth rate is in general less strongly influenced by density dependent processes, and therefore it is less likely that an interactive effect will emerge from non-interactivity on the individual level.

Conclusions

We showed that metal mixture toxicity to *D. magna* populations is in large part predictable based on the assumption of non-interactivity on the physiological level. While further validation is needed before generalizing this conclusion, our findings are in agreement with previous analyses of metal mixture toxicity, showing that strong interactive effects between metals are rare (Cedergreen, 2014) and that IA is, on average, the more adequate reference model than CA at the individual level (Nys, Versieren, et al., 2017). If confirmed by further validation, the use of DEB-IBM in mixture ecotoxicology opens up the opportunity for extrapolations that are not possible with statistical reference models, such as prediction of mixture toxicity at different food levels or exposure durations. Therefore, mechanistic effect modelling can provide considerable advantages over purely empirical models even if the predictive performance of the mechanistic model does not exceed that of empirical models. Furthermore, mechanistic models can serve as a tool for the formulation of clear and well-

623 founded hypotheses, since they point at specific processes being responsible for observed
624 phenomena.

625 Accurate predictions can be provided without using point estimates of TKTD parameters.
626 Instead, by sampling parameter values from joint posterior distributions, the uncertainty
627 associated with each estimation can be propagated. Also in terms of pMoAs, similarly
628 probable alternative models can be taken into account when generating predictions. This
629 facilitates the use of mechanistic effect modelling under uncertainty, e.g. when not all of the
630 desired data for calibration are available. However, it should raise caution when trying to
631 make generalized statements about pMoAs.

632 To explain why DEB-IBM predictions are much more accurate for 6-week density than for
633 growth rate, we suggest that relationships between individual-level processes and population-
634 level endpoints should be further illuminated. Specifically, our results suggest that
635 implementation of interactive mixture toxicity on the individual-level might be more
636 important when the goal is to predict mixture effects on population growth rates.

637 Our identified pMoAs were not in agreement with those reported in previous studies. For the
638 advancement of mechanistic effect modelling approaches, it will be important to understand
639 whether this is the result of intraspecific variability, an artifact of different model selection
640 approaches, or whether pMoAs might actually shift under toxicant exposure in a population
641 context.

642

643 ## References

644 Ashauer, R., Caravatti, I., Hintermeister, A., & Escher, B. I. (2010). Bioaccumulation kinetics of
645 organic xenobiotic pollutants in the freshwater invertebrate Gammarus pulex modeled
646 with prediction intervals. *Environ. Toxicol. Chem*. DOI: 10.1002/etc.175.
647 Ashauer, R., & Jager, T. (2018). Physiological modes of action across species and toxicants: The
648 key to predictive ecotoxicology. *Environ. Sci.: Process. Impacts*. DOI :
649 10.1039/C7EM00328E.

650 Billoir, E., Pèry, A. R. R., & Charles, S. (2007). Integrating the lethal and sublethal effects of
651 toxic compounds into the population dynamics of Daphnia magna: A combination of
652 the DEBtox and matrix population models. *Ecol. Modell. 203*:204–214.
653 Brix, K. V., Schlekat, C. E., & Garman, E. R. (2017). The mechanisms of nickel toxicity in aquatic
654 environments: An adverse outcome pathway analysis. *Environ. Toxicol. Chem.* DOI:
655 10.1002/etc.3706.
656 Cedergreen, N. (2014). Quantifying Synergy: A Systematic Review of Mixture Toxicity Studies
657 within Environmental Toxicology. *PLoS ONE*, *9*(5), e96580. DOI:
658 10.1371/journal.pone.0096580.
659 Cedergreen, N., Kudsk, P., Mathiassen, S. K., Sørensen, H., & Streibig, J. C. (2007).
660 Reproducibility of binary-mixture toxicity studies. *Environ. Toxicol. Chem.*, *26*(1). DOI:
661 10.1897/06-196R.1.
662 De Schamphelaere, K. A. C., & Janssen, C. R. (2002). A Biotic Ligand Model Predicting Acute
663 Copper Toxicity for Daphnia magna: The Effects of Calcium, Magnesium, Sodium,
664 Potassium, and pH. *Environ. Sci. Technol. DOI:* 10.1021/es000253s.
665 De Schamphelaere, K. A. C., & Janssen, C. R. (2004). Development and field validation of a
666 biotic ligand model predicting chronic copper toxicity to Daphnia magna. *Environ.*
667 *Toxicol. Chem.*, *23*(6). DOI: 10.1897/02-626.
668 De Schamphelaere, K. A. C., Unamuno, V. I. R., Tack, F. M. G., Vanderdeelen, J., & Janssen, C.
669 R. (2005). Reverse osmosis sampling does not affect the protective effect of dissolved
670 organic matter on copper and zinc toxicity to freshwater organisms. *Chemosphere*.
671 DOI: 10.1016/j.chemosphere.2004.06.039.
672 De Schamphelaere, K. A. C., Vasconcelos, F. M., Heijerick, D. G., Tack, F. M. G., Delbeke, K.,
673 Allen, H. E., & Janssen, C. R. (2003). Development and field validation of a predictive
674 copper toxicity model for the green alga Pseudokirchneriella subcapitata. *Environ.*
675 *Toxicol. Chem.* DOI: 10.1897/02-499.
676 Faust, M., Altenburger, R., Backhaus, T., Blanck, H., Boedeker, W., Gramatica, P., Hamer, V.,
677 Scholze, M., Vighi, M., & Grimme, L. H. (2003). Joint algal toxicity of 16 dissimilarly
678 acting chemicals is predictable by the concept of independent action. *Aquat. Toxicol.*–
679 DOI: 10.1016/S0166-445X(02)00133-9.

680 Gergs, A., Preuss, T. G., & Palmqvist, A. (2014). Double Trouble at High Density: Cross-Level
681 Test of Resource-Related Adaptive Plasticity and Crowding-Related Fitness. *PLoS ONE*.
682 DOI: 10.1371/journal.pone.0091503.
683 Grimm, V., Berger, U., DeAngelis, D. L., Polhill, J. G., Giske, J., & Railsback, S. F. (2010). The ODD
684 protocol: A review and first update. *Ecol. Modell.*, *221*(23). DOI:
685 10.1016/j.ecolmodel.2010.08.019.
686 Grimm, V., & Martin, B. T. (2013). Mechanistic effect modeling for ecological risk assessment:
687 Where to go from here? *IEAM*, *9*(3). DOI: 10.1002/ieam.1423.
688 Heugens, E. H. W., Tokkie, L. T. B., Kraak, M. H. S., Hendriks, A. J., Straalen, N. M. van, &
689 Admiraal, W. (2006). Population growth of Daphnia magna under multiple stress
690 conditions: Joint effects of temperature, food, and cadmium. *Environ. Toxicol. Chem.*
691 DOI: 10.1897/05-294R.1.
692 Hochmuth, J. D., Asselman, J., & De Schamphelaere, K. A. C. (2014). Are interactive effects of
693 harmful algal blooms and copper pollution a concern for water quality management?
694 *Water Res.* DOI: 10.1016/j.watres.2014.03.041.
695 Jager, T. (2011). Some Good Reasons to Ban ECx and Related Concepts in Ecotoxicology.
696 *Environ. Sci. Technol.* DOI: 10.1021/es2030559.
697 Jager, T., Albert, C., Preuss, T. G., & Ashauer, R. (2011). General Unified Threshold Model of
698 Survival—A Toxicokinetic-Toxicodynamic Framework for Ecotoxicology. *Environ. Sci.*
699 *Technol*. DOI : 10.1021/es103092a.
700 Jager, T., Heugens, E. H. W., & Kooijman, S. A. L. M. (2006). Making Sense of Ecotoxicological
701 Test Results: Towards Application of Process-based Models. *Ecotoxicology*. DOI:
702 10.1007/s10646-006-0060-x.
703 Jager, T., Vandenbrouck, T., Baas, J., De Coen, W. M., & Kooijman, S. A. L. M. (2010). A biology-
704 based approach for mixture toxicity of multiple endpoints over the life cycle.
705 *Ecotoxicology*. DOI: 10.1007/s10646-009-0417-z.
706 Jonker, M. J., Svendsen, C., Bedaux, J. J. M., Bongers, M., & Kammenga, J. E. (2005).
707 Significance testing of synergistic/antagonistic, dose level-dependent, or dose ratio-
708 dependent effects in mixture dose-response analysis. *Environ. Toxicol. Chem.* DOI:
709 10.1897/04-431R.1.

710 Kilham, S. S., Kreeger, D. A., Lynn, S. G., Goulden, C. E., & Herrera, L. (1998). COMBO: A defined
711 freshwater culture medium for algae and zooplankton. *Hydrobiologia*. DOI:
712 10.1023/A:1003231628456.
713 Kooijman, S. A. L. M. (2010). *Dynamic Energy Budget Theory for Metabolic Organisation*.
714 Cambridge University Press.
715 Kooijman, S. A. L. M., & Bedaux, J. J. M. (1996). *The analysis of aquatic toxicity data*. VU
716 University Press.
717 Kooijman, S.A. L. M., & Gergs, A. (2019). Daphnia magna. In *AmP*.
718 https://www.bio.vu.nl/thb/deb/deblab/add_my_pet/entries_web/Daphnia_magna/
719 Daphnia_magna_res.html.
720 Kooijman, S. A. L. M., Sousa, T., Pecquerie, L., Meer, J. V. D., & Jager, T. (2008). From food-
721 dependent statistics to metabolic parameters, a practical guide to the use of dynamic
722 energy budget theory. *Biol. Rev.* DOI: 10.1111/j.1469-185X.2008.00053.x.
723 Lampert, W. (1974). A method for determining food selection by zooplankton. *Limnol.*
724 *Oceanogr.*, *19*(6), 995–998. DOI: 10.4319/lo.1974.19.6.0995.
725 Loewe, S., & Muischnek, H. (1926). Über Kombinationswirkungen. *Naunyn-Schmiedebergs*
726 *Archiv für experimentelle Pathologie und Pharmakologie*. DOI: 10.1007/BF01952257.
727 Loureiro, S., Svendsen, C., Ferreira, A. L. G., Pinheiro, C., Ribeiro, F., & Soares, A. M. V. M.
728 (2010). Toxicity of three binary mixtures to Daphnia magna: Comparing chemical
729 modes of action and deviations from conceptual models. *Environ. Toxicol. Chem.* DOI:
730 10.1002/etc.198.
731 Marques, G. M., Lika, K., Augustine, S., Pecquerie, L., & Kooijman, S. A. L. M. (2019). Fitting
732 multiple models to multiple data sets. *J. Sea Res.* DOI: 10.1016/j.seares.2018.07.004
733 Martin, B. T., Jager, T., Nisbet, R. M., Preuss, T. G., Hammers-Wirtz, M., & Grimm, V. (2013).
734 Extrapolating ecotoxicological effects from individuals to populations: A generic
735 approach based on Dynamic Energy Budget theory and individual-based modeling.
736 *Ecotoxicology*. DOI: 10.1007/s10646-013-1049-x.
737 Martin, B. T., Zimmer, E. I., Grimm, V., & Jager, T. (2012). Dynamic Energy Budget theory meets
738 individual-based modelling: A generic and accessible implementation. *Methods Ecol.*
739 *Evol.* DOI: 10.1111/j.2041-210X.2011.00168.x.
740 Nys, C., Asselman, J., Hochmuth, J., Janssen, C. R., Blust, R., Smolders, E., & De Schamphelaere,
741 K. A. C. (2015). Mixture toxicity of Nickel and Zinc to Daphnia magna is noninteractive

742 at low effect sizes but becomes synergistic at high effect sizes. *Environ. Toxicol. Chem.*
743 DOI: 10.1002/etc.2902.
744 Nys, C., Janssen, C. R., & De Schamphelaere, K. A. C. (2017). Development and validation of a
745 metal mixture bioavailability model (MMBM) to predict chronic toxicity of Ni-Zn-Pb
746 mixtures to Ceriodaphnia dubia. *Environ. Pollut.* DOI: 10.1016/j.envpol.2016.10.104.
747 Nys, C., Versieren, L., Cordery, K. I., Blust, R., Smolders, E., & De Schamphelaere, K. A. C. (2017).
748 Systematic Evaluation of Chronic Metal-Mixture Toxicity to Three Species and
749 Implications for Risk Assessment. *Environ. Sci. Technol.* DOI : 10.1021/acs.est.6b05688.
750 OECD. (2012). *Test No. 211: Daphnia magna Reproduction Test*. Organisation for Economic Co-
751 operation and Development, Paris, France.
752 Pereira, C. M. S., Vlaeminck, K., Viaene, K., & Schamphelaere, K. A. C. D. (2019). The
753 Unexpected Absence of Nickel Effects on a Daphnia Population at 3 Temperatures is
754 Correctly Predicted by a Dynamic Energy Budget Individual-Based Model. *Environ.*
755 *Toxicol. Chem.* DOI: 10.1002/etc.4407.
756 Pieters, B. J., Jager, T., Kraak, M. H. S., & Admiraal, W. (2006). Modeling responses of Daphnia
757 magna to pesticide pulse exposure under varying food conditions: Intrinsic versus
758 apparent sensitivity. *Ecotoxicology*. DOI: 10.1007/s10646-006-0100-6.
759 Van Regenmortel, T., Nys, C., Janssen, C. R., Lofts, S., & Schamphelaere, K. A. C. D. (2017).
760 Comparison of four methods for bioavailability-based risk assessment of mixtures of
761 Cu, Zn, and Ni in freshwater. *Environ. Toxicol. Chem.* DOI: 10.1002/etc.3746.
762 Sisson, S. A., Fan, Y., & Tanaka, M. M. (2007). Sequential Monte Carlo without likelihoods.
763 *PNAS*. DOI: 10.1073/pnas.0607208104.
764 Smith, R., Martell, A., & Motekaitis, R. (2004). NIST critically selected stability constants of
765 metal complexes database. In *NIST STand Ref Database 46.(Version 8.0)*. National
766 Institute of Standard and Technology. https://www.nist.gov/document-14894.
767 Tipping, E., Lofts, S., & Sonke, J. E. (2011). Humic Ion-Binding Model VII: A revised
768 parameterisation of cation-binding by humic substances. *Environ. Chem.* DOI:
769 10.1071/EN11016.
770 Toni, T., Welch, D., Strelkowa, N., Ipsen, A., & Stumpf, M. P. H. (2009). Approximate Bayesian
771 computation scheme for parameter inference and model selection in dynamical
772 systems. *J. R. Soc. Interface*. DOI: 10.1098/rsif.2008.0172.

van der Vaart, E., Beaumont, M. A., Johnston, A. S. A., & Sibly, R. M. (2015). Calibration and evaluation of individual-based models using Approximate Bayesian Computation. *Ecol. Modell.* DOI: 10.1016/j.ecolmodel.2015.05.020.

Versieren, L., Smets, E., De Schamphelaere, K., Blust, R., & Smolders, E. (2014). Mixture toxicity of copper and zinc to barley at low level effects can be described by the Biotic Ligand Model. *Plant and Soil*. DOI: 10.1007/s11104-014-2117-6.

Vlaeminck, K., Viaene, K. P. J., Sprang, P. V., & Schamphelaere, K. A. C. D. (2021). Development and Validation of a Mixture Toxicity Implementation in the Dynamic Energy Budget–Individual-Based Model: Effects of Copper and Zinc on Daphnia magna Populations. *Environ. Toxicol. Chem.* DOI: 10.1002/etc.4946.

Tables

Table 1 Mean and standard deviation with sample sizes of measured test media physicochemistry

T (°C)	pH	Na_a	Mg_a	K_a	Ca_a	DOC_a
19.4 (0.9, N=12)	7.6 (0.6, N=268)	27.1 (2.5, N=404)	5.01 (0.24, N=404)	4.26 (1.70, N=404)	13.8 (0.8, N=404)	7.32 (0.84, N=404)

[a] mg L^{-1}

Table 2 Estimated DEB parameters for D. magna. Point estimates are the particle with the best fit. Credible Limits (CL) indicate the corresponding percentile of the marginal posterior distribution

PARAMETER	UNIT	DESCRIPTION	Add-my-pet reported value (Kooijman & Gergs, 2019)	ESTIMATE	CL_5	CL_{95}
p_{Am}	$\frac{J}{cm^2 \times day}$	maximum specific assimilation rate	313.2	260.4	264.0	308.1
F_m	$\frac{L}{cm^2 \times day}$	filtration rate	30.17	10.0	8.6	11.8
$\kappa_{E,X}$	$\frac{J}{algal\ cell}$	assimilation efficiency	not reported	3.7×10^{-6}	3.1×10^{-6}	4.1×10^{-6}
m_e	-	reserve density-related mortality	not reported	0.41	0.32	0.62

790

791 Table 3 Deviation parameter a (Equation 11) per treatment, endpoint and reference model.

treatment	endpoint	$\sum TU_{EC50}$[a]	model	a	CL_{5} [b]	CL_{95} [b]	observed[c]	predicted by null model	p-value[d]	S/A[e]
Mix1	r	0.08	IA	6.69	6.63	6.77	0.98 (0.03)	0.75	<0.0025	A
	K	0.21		31.6	31.3	31.9	0.89 (0.03)	0.8	<0.0025	A
	r	0.08	CA	-5.3	-5.36	-5.24	0.98 (0.03)	1.0	<0.0025	S
	K	0.21		-65.9	-66.6	-65	0.89 (0.03)	0.99	<0.0025	S
Mix2	r	0.19	IA	-1.35	-1.36	-1.33	0.9 (0.12)	0.95	<0.0025	S
	K	0.42		-108	-110	-107	0.81 (0.08)	1	<0.0025	S
	r	0.19	CA	-3.81	-3.85	-3.77	0.9 (0.12)	0.99	<0.0025	S
	K	0.42		-19.6	-19.8	-19.3	0.81 (0.08)	0.94	<0.0025	S
Mix3	r	0.56	IA	40.3	34.5	118	1.01 (0.11)	0.78	<0.0025	A
	K	1.21		25.2	24.9	25.5	0.71 (0.05)	0.51	<0.0025	A
	r	0.56	CA	17	11.5	17.7	1.01 (0.11)	0.86	<0.0025	A
	K	1.21		22.9	22.7	23.2	0.71 (0.05)	0.35	<0.0025	A
Mix4	r	1.70	IA	-1.77	-1.79	-1.75	0.31 (0.62)	0.48	<0.0025	S
	K	3.21		-154.51	-154.51	-154.51	0.0 (0.0)	0.04	<0.0025	S
	r	1.70	CA	1.34	1.32	1.36	0.31 (0.62)	0.08	<0.0025	A
	K	3.21		-81.2	-87.7	-74.39	0.0 (0.0)	0.02	<0.0025	S

Mix5	r	8.6	IA	NaN_f	NaN_f	NaN_f	0.0 (0.0)	0	-	-
	K	13.3		NaN_f	NaN_f	NaN_f	0.0 (0.0)	0	-	-
	r	8.6	CA	NaN_f	NaN_f	NaN_f	0.0 (0.0)	0	-	-
	K	13.3		NaN_f	NaN_f	NaN_f	0.0 (0.0)	0	-	-

792 [a] Sum of toxic units based on median effect concentration with respect to the corresponding
793 endpoint.

794 [b] Percentile of marginal posterior distribution of a.

795 [c] Mean and standard deviation of control-normalized responses; N=4 for each entry

796 [d] Derived by nested F-test.

797 [e] S=Synergism, A=Antagonism

798 [f] NaN = "Not a Number". Deviation parameter could not be determined if all observed and
799 predicted responses are equal to 0.

800

801 Table 4 Model performance per endpoint. SSE is the sum of squared errors between
802 predicted and observed control-normalized values.

endpoint	model	R^2_a	SSE_b
r	IA_c	0.70	1.79
	CA_c	0.75	1.58
	IBM	0.73	1.64
K	IA_c	0.92	0.44
	CA_c	0.90	0.65
	IBM	0.97	0.17

803

804 [a] Linear regression between predicted and observed control-normalized responses in the
805 mixture treatments.

806 [b] Sum of Squared Errors between predicted and observed control-normalized responses.

807 $_c$ Null model (no deviation parameter)

808

809

810 ## Figures

811

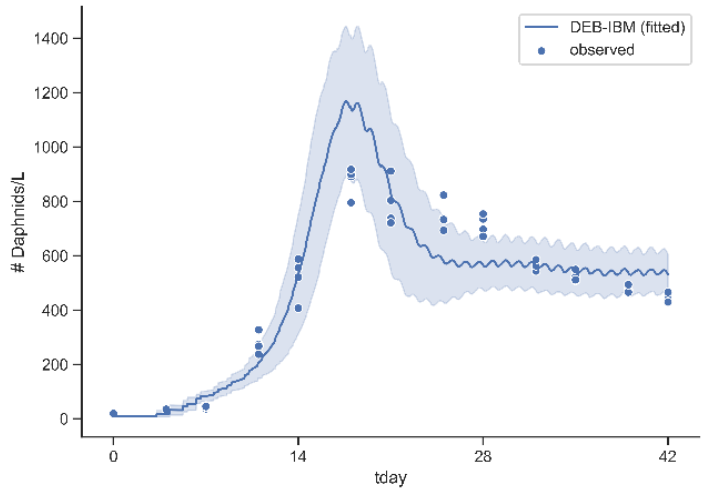

812

813 Figure 1 Fitted and observed population dynamics in the control. Lines and ribbons show
814 mean and standard deviation of predictions generated from 100 posterior samples.

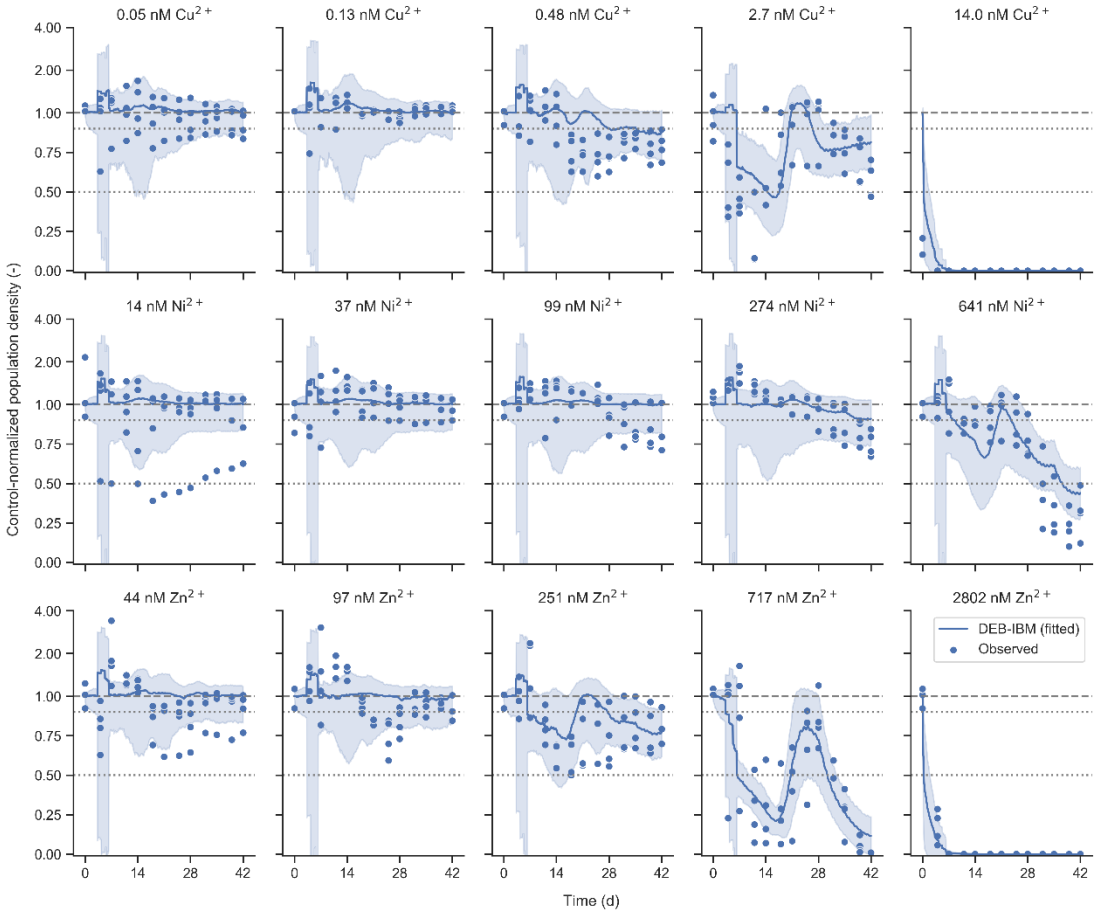

Figure 2 Fitted and observed control-normalized responses of population density in single-metal treatments. Responses above one (dashed gray line) are shown on a logarithmic scale. Fitted values are the result of evaluating the DEB-IBM for 100 samples from the corresponding posterior distribution of TKTD parameters, as well as the posterior distribution of DEB parameters. Lines and shaded areas indicate the mean and standard deviation of predicted responses.

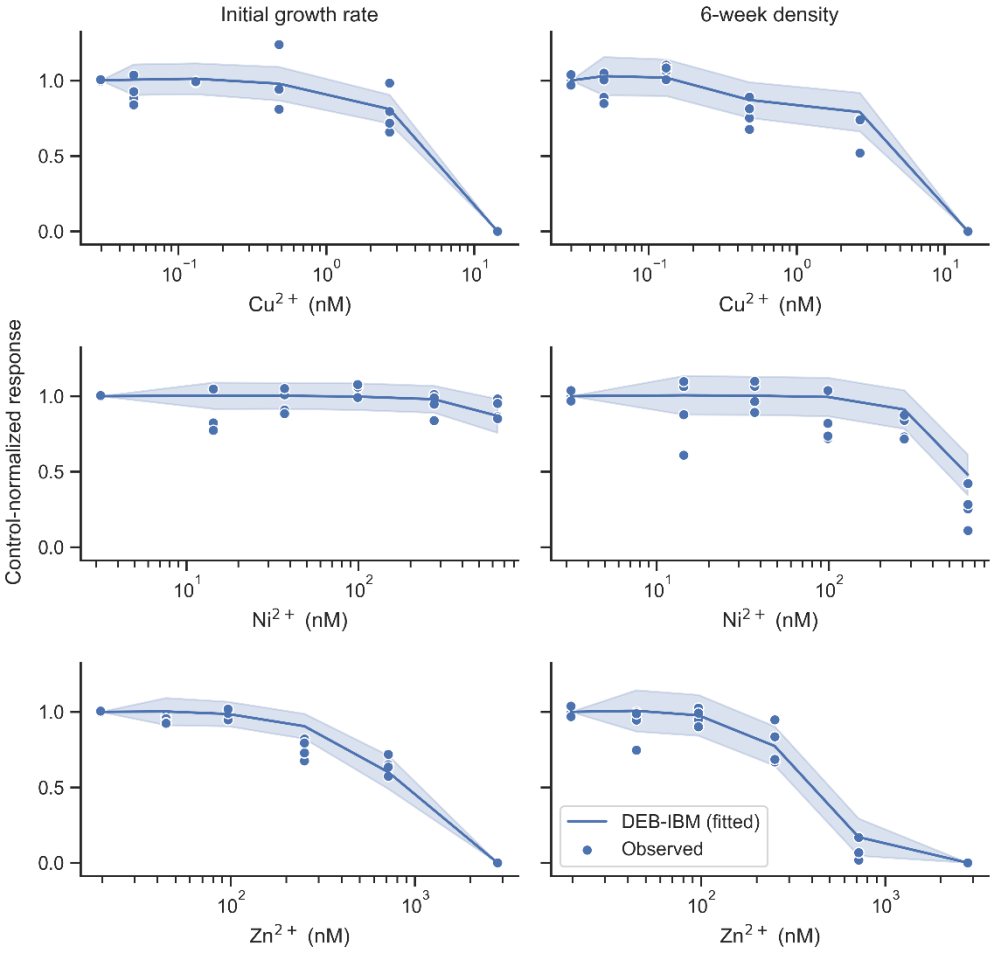

Figure 3 Observed and IBM-predicted control-normalized responses of initial growth rate and 6-week density in the single-metal treatments, after fitting the DEB-IBM to time series of control-normalized population densities in the single-metal treatments. Lines and shaded areas indicate mean and standard deviation of predicted responses based on 100 posterior samples.

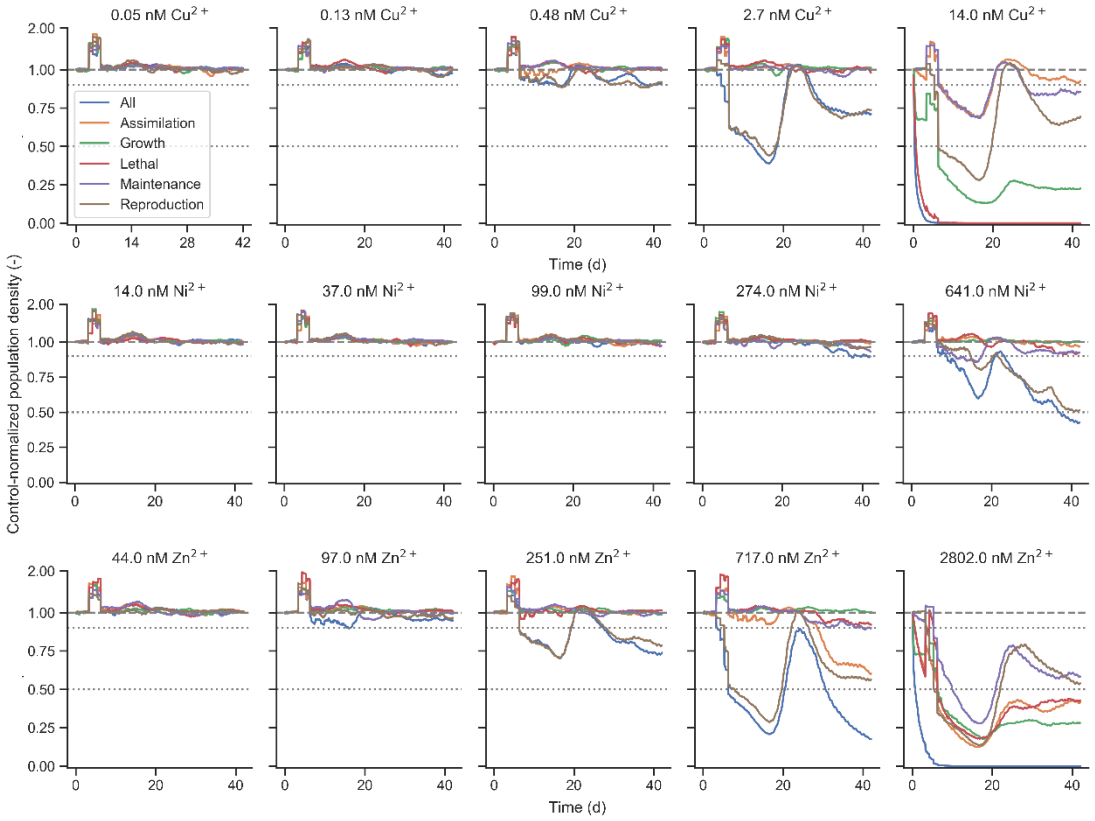

Figure 4 Predicted control-normalized response of population density over time, if all or only one toxicity component are simulated. In the model, effects on reproduction efficiency caused most of the effect across metals at low and intermediate effect concentrations. Responses above one (dashed line) are shown on a log-scale. Dotted lines indicate the 10% and 50% effect levels, respectively.

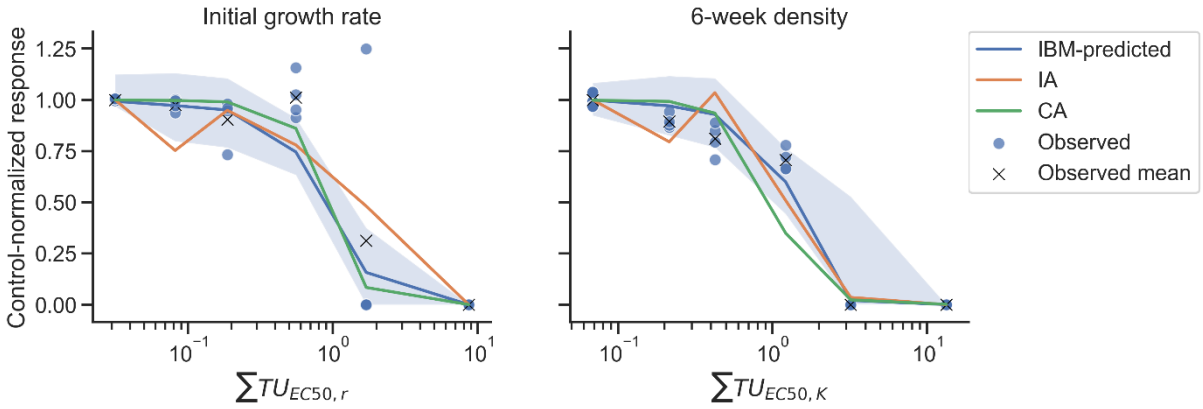

Figure 5 Observed and model-predicted control-normalized responses of initial growth rate and 6-week density in the mixture treatments. Toxic units are calculated based on the corresponding EC50s of individual metals, which were obtained by fitting log-logistic curves. "IA" and "CA" are empirical models applied on the population-level. "IBM-predicted" are DEB-IBM predicted values based on calibration with single-metal toxicity data and IA on the physiological level.

Figure 6 Observed and model-predicted control-normalized responses of initial growth rate and 6-week density in the mixture treatments. Responses above one (dashed gray line) are shown on a logarithmic scale. Toxic units are calculated based on the corresponding EC50s of individual metals, which were obtained by fitting log-logistic curves. “IA” and “CA” are empirical models applied on the population-level. “IBM-predicted” are DEB-IBM predicted values based on calibration with single-metal toxicity data and IA on the physiological level. Dotted gray lines indicate the 10% and 50% effect levels, respectively.

Supporting Information

ICP-OES detection limits and quality control

SI Table 1 ICP-OES Method Detection Limits (MDL) and Limits of Quantification (LOQ) of measured cations.

	Cu	**Ni**	**Zn**	**Ca**	**Mg**	**Na**	**K**
Position Torch	Axial	Axial	Axial	Radial	Radial	Radial	Radial
MDL ($\mu g\ L^{-1}$)	2.0	1.2	0.5	15	15	30	30
LOQ ($\mu g\ L^{-1}$)	5.0	4.0	2.0	50	50	100	100

SI Table 2 Recovery percentages for major cations, based on the reference material Cranberry-05 (Environment Canada). Shown are ranges of determined recovery percentages based on a total of 7 measurements.

Element	**Recovery percentage**
Na	102-108%
Mg	92-103%
K	96-106%
Ca	92-95%

SI Table 3 Recovery percentages for minor cations, based on two different reference materials (Environment Canada). Shown are ranges of determined recovery percentages based on a total of 4 measurements for each reference material.

Reference material	**Element**	**Recovery percentage**
TM-25.5	Cu	97-101%
	Ni	91-102%
	Zn	105-107%
TMDA-70.2	Cu	95-98%
	Ni	95-107%
	Zn	101-102%

Overview of the modelling scheme

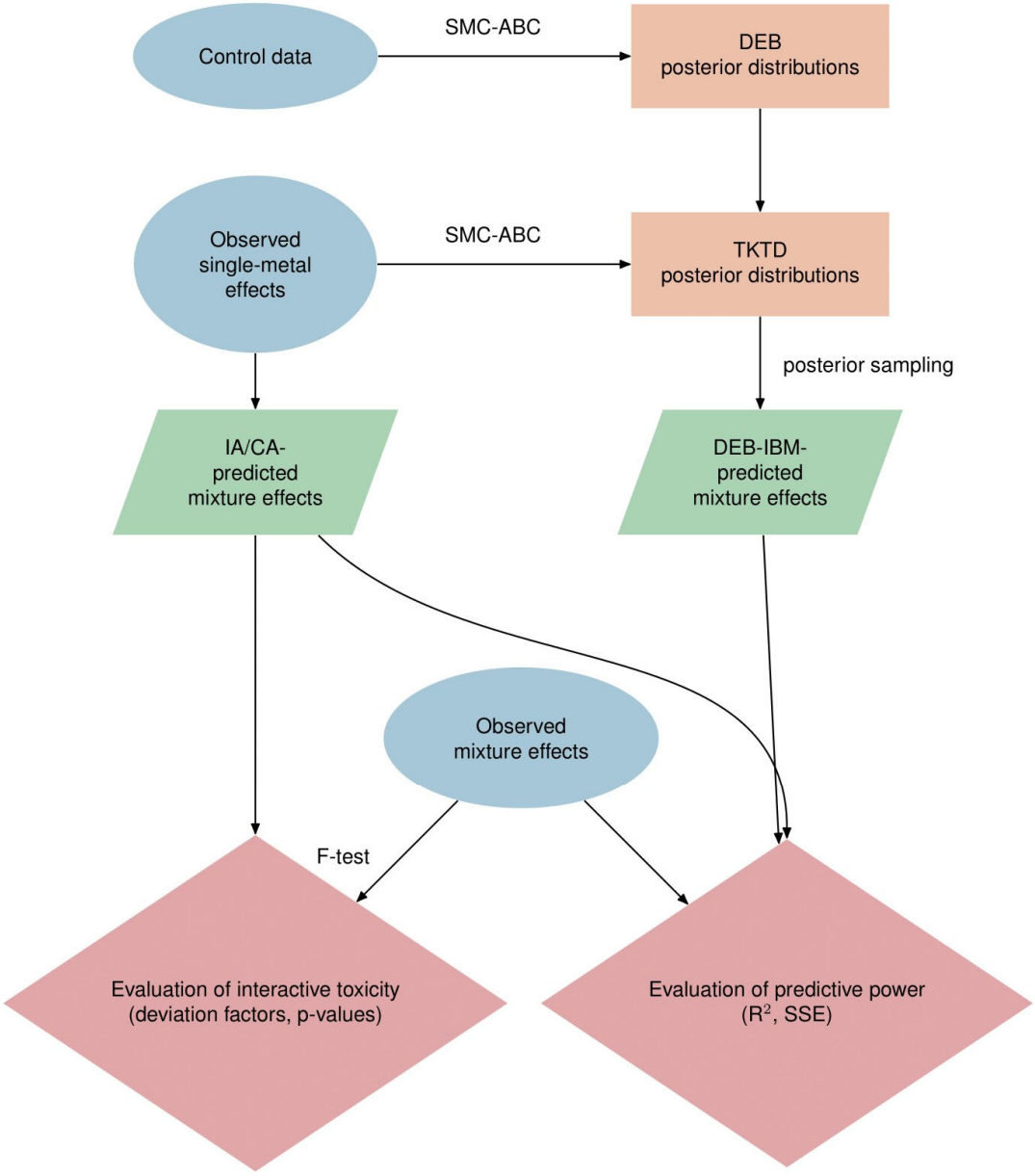

SI Figure 1 Schematic representation of modelling and statistical analysis.

Sequential Monte Carlo Approximate Bayesian Computation (SMC-ABC) scheme

For estimation of DEB parameters, we used the function SMCABC (gpABC package in Julia) with Euclidean distance as loss function. gpABC implements the algorithm by Toni et al. (2009).

Estimation of TKTD parameters proved more intricate. For sake of transparency, we implemented a custom Sequential Monte Carlo Approximate Bayesian Computation (SMC-ABC) scheme for TKTD parameter estimation, loosely based on the algorithms provided by Toni et al. (2009) and Sisson et al. (2007). As all ABC-based approaches, it does not involve explicit calculation of likelihood. Instead, the loss function is used as a proxy for the likelihood and Bayes' rule is applied implicitly. The scheme proceeds as follows:

1. Sample a particle θ (i.e. combination of parameter values) from prior distributions.
2. Simulate the model with θ as input variable and evaluate the loss function $\rho(M(\theta), D)$ for model $M(\theta)$ and data D.
3. Repeat steps 1-2 n times.
4. Steps 1-3 result in a population of particles θ_i and corresponding losses ρ_i. Compute the 20th percentile of the distribution of ρ_i, and select particles θ^* whose distance falls below that percentile.
5. Repeat steps 1-4 k times, sampling from the previous population θ_i^* of particles instead of the initial prior, with sampling weights equal to ρ^{-1}. In addition, multiply each sampled value by a random perturbation factor $e^{Norm(0,0.1)}$.

For estimating TKTD parameters, we set n to 250 and k to 20. These settings are a compromise between keeping computation times within acceptable ranges and exploring the possible parameter space.

Note that in contrast to classic rejection ABC, this scheme can result in the parameter estimates drifting outside the boundaries of the initial prior distributions.

As distance function we used a symmetric bounded function (Marques et al., 2019). By using a percentile of ρ_i as criterion to accept particles, we omitted the step of defining a distance schedule (i.e. a vector of absolute values of the loss function as successive criterion for particle acceptance). Application of a perturbation factor avoids the exact parameter values to be constrained by the first set of samples.

References

Marques, G. M., Lika, K., Augustine, S., Pecquerie, L., & Kooijman, S. A. L. M. (2019). Fitting multiple models to multiple data sets. Journal of Sea Research, 143, 48–56. https://doi.org/10.1016/j.seares.2018.07.004

Sisson, S. A., Fan, Y., & Tanaka, M. M. (2007). Sequential Monte Carlo without likelihoods. Proceedings of the National Academy of Sciences, 104(6), 1760–1765. https://doi.org/10.1073/pnas.0607208104

Toni, T., Welch, D., Strelkowa, N., Ipsen, A., & Stumpf, M. P. H. (2009). Approximate Bayesian computation scheme for parameter inference and model selection in dynamical systems. Journal of The Royal Society Interface, 6(31), 187–202. https://doi.org/10.1098/rsif.2008.0172

Implementation of physiological Modes of Action

Stress functions were applied to DEB parameters and state variables according to the corresponding physiological Mode of Action (pMoA). For combined effects of metals via the same pMoA, the stress functions were calculated individually, then combined multiplicatively.

SI Table 4 pMoAs and their corresponding effect on DEB parameters and state variables. Mentioned parameters are energy investment ratio g $(-)$, somatic maintenance rate constant $\dot{k}_M$ (day^{-1}), maturity maintenance rate constant $\dot{k}_J$ (day^{-1}) and reproduction efficiency κ_R $(-)$. S_A is the scaled assimilation flux (cm^2). $S_{i,j}$ is stress caused by stressor i with resepect to pMoA j. For detailed explanations of parameters, see Kooijman (2010). "→ " denotes assignment.

pMoA	**stressed value**
Increase in growth costs (G)	$g \rightarrow g(1 + S_{i,G})$
	$\dot{k}_M \rightarrow \dot{k}_M \frac{1}{1 + S_{i,G}}$
Increase in maintenance costs (M)	$\dot{k}_M \rightarrow \dot{k}_M(1 + S_{i,M})$
	$\dot{k}_J \rightarrow \dot{k}_J(1 + S_{i,M})$
Decrease in assimilation flux (A)	$S_A \rightarrow S_A(1 - S_{i,A})$
Decrease in reproduction efficiency (R)	$\kappa_R \rightarrow \kappa_R(1 - S_{i,R})$

Physicochemistry

pH

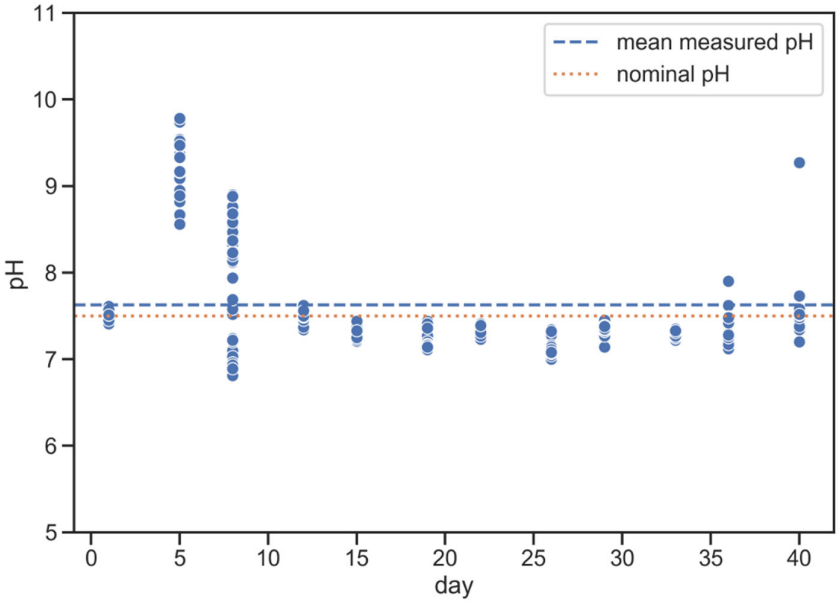

SI Figure 2 Measured pH over time. pH increased in the first week, likely due to photosynthetic activity of added algae, but fell back when exponential growth of Daphnia populations started.

Derivation of exposure concentration time-series

Because exposure concentrations varied over time, we used the WHAM VII-predicted free ion activities (based on measured concentrations) to derive time-series of free ion activities, which were in turn used as input for the DEB-IBM simulations. In each week, samples of new and old media were taken. Free ion activities systematically differed between new (=directly after 25% renewal) and old (=right before 25% renewal) media, and tended to overall increase during the experiment. We therefore implemented a procedure to derive the time series from pairs of measurements.

For illustration purposes, consider the following random example:

time (days)	medium type	$[Cu^{2+}]$
7	new	1.7
	old	0.2

14	new	2.2
	old	1.5

Shown are free ion activities of Copper in a given treatment, at two successive time-points of measurement in the experiment. Assume we want to derive the concentration which will be used as input for the DEB-IBM simulation from day 7 to day 14. The concentration in the old medium at day 7 should be irrelevant for this, since the populations will be exposed to the concentration in the new medium from day 7 on. The same applies to the concentration in the new medium at day 14. The concentration to which the populations are in fact exposed to between day 7 and day 14 should be best described by the concentration in the *new* medium at day 7 and the *old* medium at day 14. To not complicate the computation any further, we used the average between these two values to obtain the DEB-IBM input between day 7 and day 14 for the given treatment, i.e. (1.7 nM+1.5 nM)/2 = 1.6nM. Or in general terms: The concentration used between two time-points of measurement, t1 and t2, was the average between the new concentration at t1 and the old concentration at t2. Special cases were given by the first time-point (day 0) and last time-point (day 42 or day of extinction of the last population surviving in the given treatment), where only the concentration in the new medium and in the old medium were taken into account, respectively.

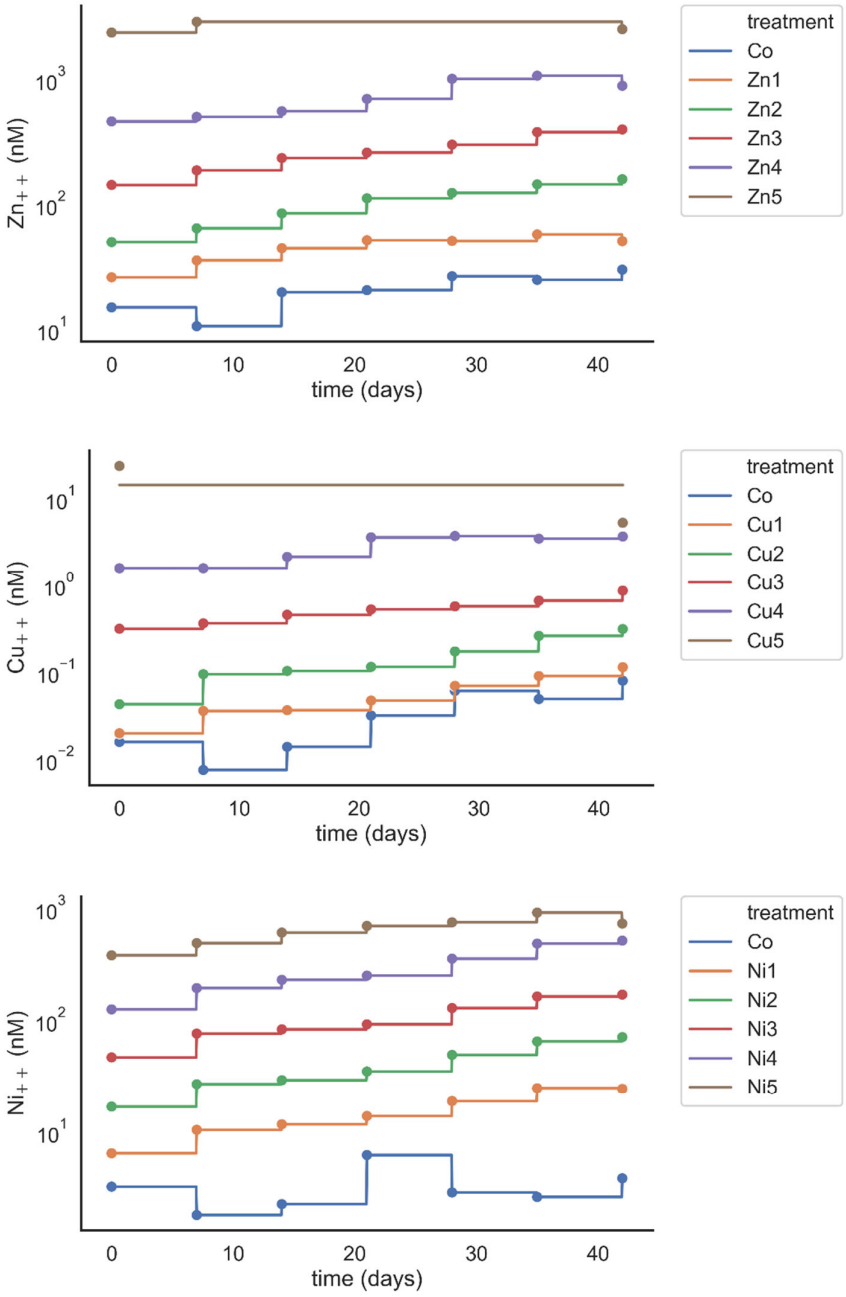

SI Figure 3 Time-series of free ion activities used for simulation of single-metal exposures.

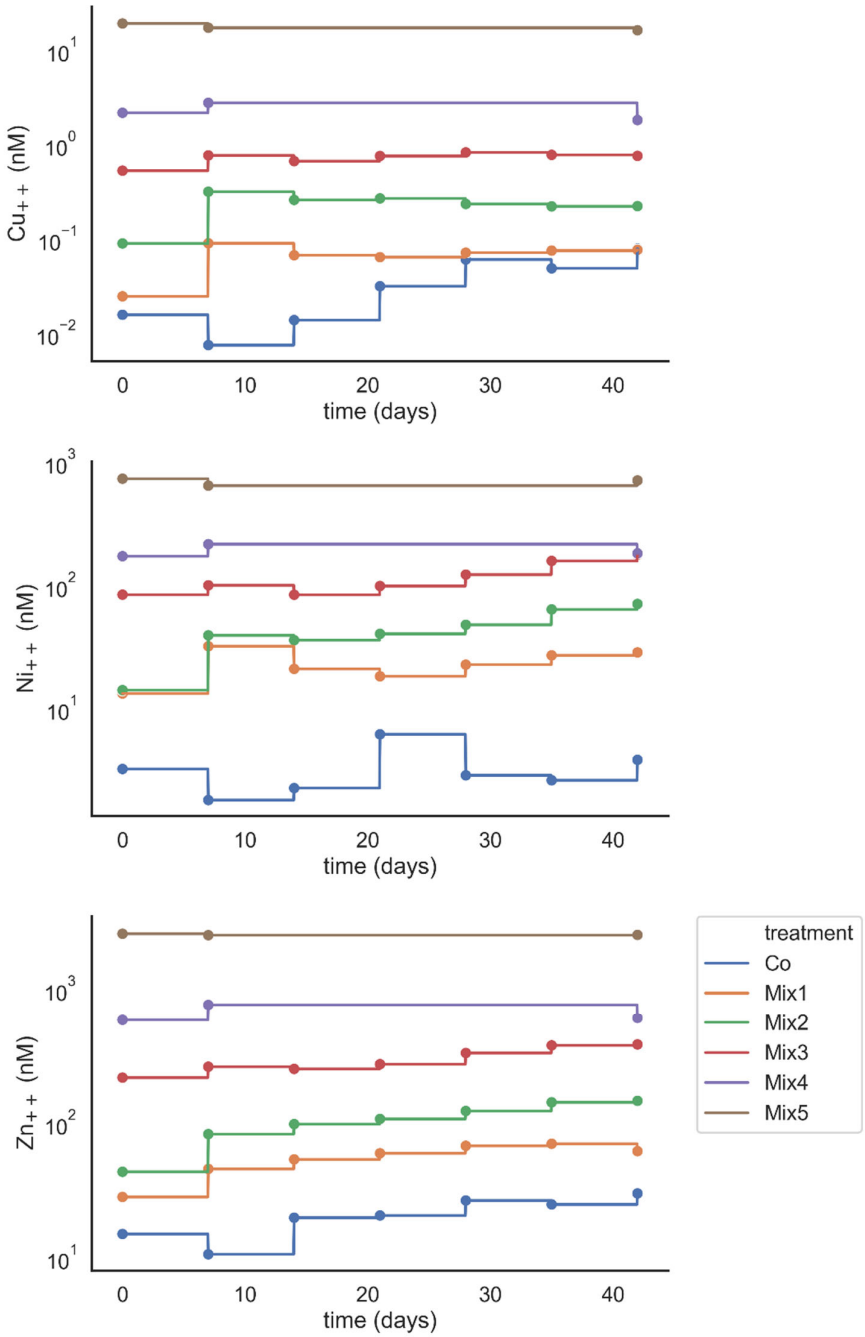

SI Figure 4 Time-series of free ion activities used for simulation of mixture exposure.

130

131

132

133

SI Table 5 Mean measured dissolved metal concentrations per treatment, expressed in µg L^{-1} and nM. Standard deviations and sample sizes are given in brackets. Limits of quantification (LOQ) for Cu, Ni and Zn were 5, 4 and 2 µg L^{-1} respectively.

treatment	Cu (µg L^{-1})		Cu (nM)		Ni (µg L^{-1})		Ni (nM)		Zn (µg L^{-1})		Zn (nM)	
	nom.	mes.	nom.	mes.	nom.	mes.	nom.	mes.	nom.	mes.	nom.	mes.
Co	0.254	5.82 (2.94, N=33)	4	91.7 (46.2, N=33)	0	<LOQ (N=33)	0	<LOQ (N=33)	5.23	9.82 (3.01, N=33)	80	150.0 (46.0, N=33)
Cu1	5	8.08 (2.49, N=33)	78.7	127.0 (39.1, N=33)	0	<LOQ (N=33)	0	<LOQ (N=33)	5.23	8.3 (2.08, N=33)	80	127.0 (31.9, N=33)
Cu2	13	14.0 (2.97, N=33)	205	220.0 (46.7, N=33)	0	<LOQ (N=33)	0	<LOQ (N=33)	5.23	7.65 (2.45, N=33)	80	117.0 (37.5, N=33)
Cu3	35	28.6 (5.29, N=33)	551	450.0 (83.3, N=33)	0	<LOQ (N=33)	0	<LOQ (N=33)	5.23	7.59 (2.6, N=33)	80	116.0 (39.7, N=33)
Cu4	94	65.8 (12.0, N=33)	1480	1040.0 (188.0, N=33)	0	<LOQ (N=33)	0	<LOQ (N=33)	5.23	8.04 (1.94, N=33)	80	123.0 (29.7, N=33)
Cu5	250	178.0 (58.8, N=20)	3930	2800.0 (926.0, N=20)	0	<LOQ (N=20)	0	<LOQ (N=20)	5.23	6.58 (1.74, N=20)	80	101.0 (26.6, N=20)
Ni1	0.254	<LOQ (N=33)	4	<LOQ (N=33)	5	4.78 (1.95, N=33)	85.2	81.4 (33.1, N=33)	5.23	10.2 (2.04, N=33)	80	156.0 (31.3, N=33)
Ni2	0.254	<LOQ (N=33)	4	<LOQ (N=33)	13	12.1 (4.39, N=33)	221	207.0 (74.8, N=33)	5.23	8.78 (1.82, N=33)	80	134.0 (27.8, N=33)
Ni3	0.254	<LOQ (N=33)	4	<LOQ (N=33)	35	32.6 (9.98, N=33)	596	555.0 (170.0, N=33)	5.23	9.02 (1.68, N=33)	80	138.0 (25.6, N=33)
Ni4	0.254	<LOQ (N=33)	4	<LOQ (N=33)	94	88.5 (29.8, N=33)	1600	1510.0 (507.0, N=33)	5.23	9.12 (2.37, N=33)	80	139.0 (36.3, N=33)
Ni5	0.254	<LOQ (N=33)	4	<LOQ (N=33)	250	221.0 (65.8, N=33)	4260	3760.0 (1120.0, N=33)	5.23	8.33 (2.77, N=33)	80	127.0 (42.4, N=33)
Zn1	0.254	<LOQ (N=33)	4	<LOQ (N=33)	0	<LOQ (N=33)	0	<LOQ (N=33)	15	19.2 (4.39, N=33)	229	293.0 (67.2, N=33)
Zn2	0.254	<LOQ (N=33)	4	<LOQ (N=33)	0	<LOQ (N=33)	0	<LOQ (N=33)	40	38.8 (15.7, N=33)	612	593.0 (240.0, N=33)
Zn3	0.254	<LOQ (N=33)	4	<LOQ (N=33)	0	<LOQ (N=33)	0	<LOQ (N=33)	106	90.3 (29.3, N=33)	1620	1380.0 (448.0, N=33)
Zn4	0.254	5.51 (7.18, N=33)	4	86.7 (113.0, N=33)	0	<LOQ (N=33)	0	<LOQ (N=33)	282	246.0 (89.1, N=33)	4310	3760.0 (1360.0, N=33)
Zn5	0.254	<LOQ (N=21)	4	<LOQ (N=21)	0	<LOQ (N=21)	0	<LOQ (N=21)	750	573.0 (49.7, N=21)	11500	8760.0 (760.0, N=21)

Mix1	5	8.44 (1.17, N=33)	78.7	133.0 (18.4, N=33)	5	9.04 (1.63, N=33)	85.2	154.0 (27.8, N=33)	15	22.7 (7.46, N=33)	229	348.0 (114.0, N=33)
Mix2	13	17.8 (2.59, N=33)	205	280.0 (40.7, N=33)	13	14.9 (4.43, N=33)	221	253.0 (75.5, N=33)	40	37.2 (13.4, N=33)	612	569.0 (204.0, N=33)
Mix3	35	29.7 (5.6, N=33)	551	467.0 (88.1, N=33)	35	34.2 (9.2, N=33)	596	583.0 (157.0, N=33)	106	90.1 (20.6, N=33)	1620	1380.0 (316.0, N=33)
Mix4	94	54.3 (23.3, N=18)	1480	854.0 (367.0, N=18)	94	68.9 (23.4, N=18)	1600	1170.0 (398.0, N=18)	282	202.0 (70.7, N=18)	4310	3090.0 (1080.0, N=18)
Mix5	250	174.0 (34.4, N=18)	3930	2740.0 (542.0, N=18)	250	225.0 (3.56, N=18)	4260	3840.0 (60.7, N=18)	750	651.0 (14.6, N=18)	11500	9950.0 (224.0, N=18)

136

137

138

139

140

141

Results of TKTD parameter estimation

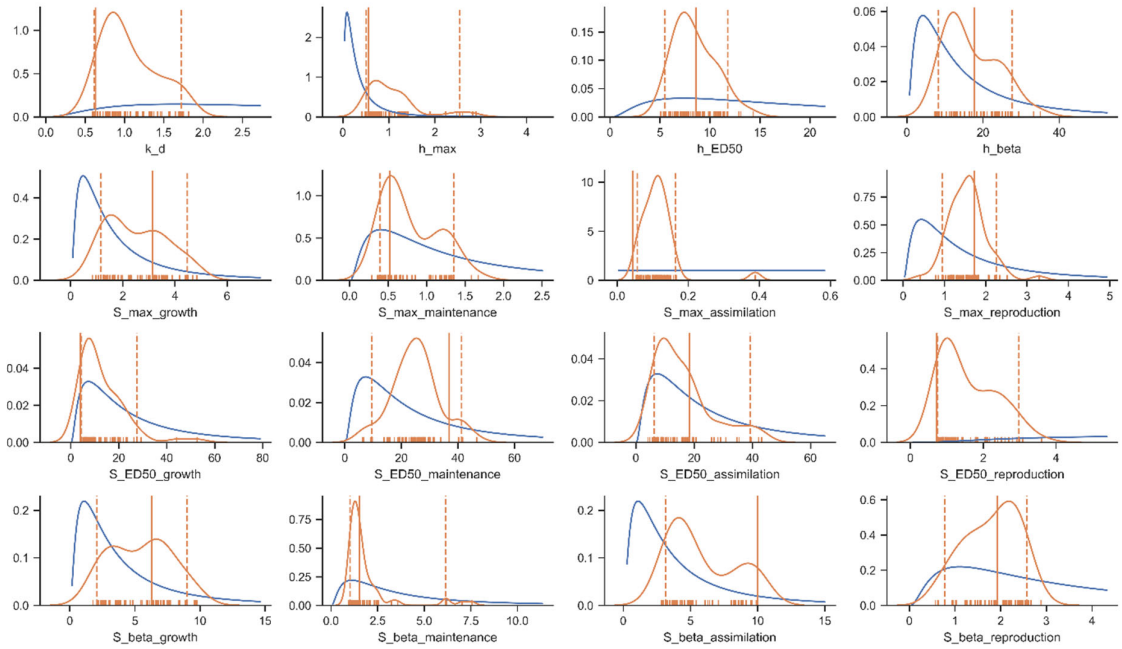

SI Figure 5 Prior (blue) and posterior (orange) probability density of TKTD parameters for Copper. Vertical bars indicate marginal 90% credible intervals. Point estimates can differ from the value associated with the highest probability density due to covariance.

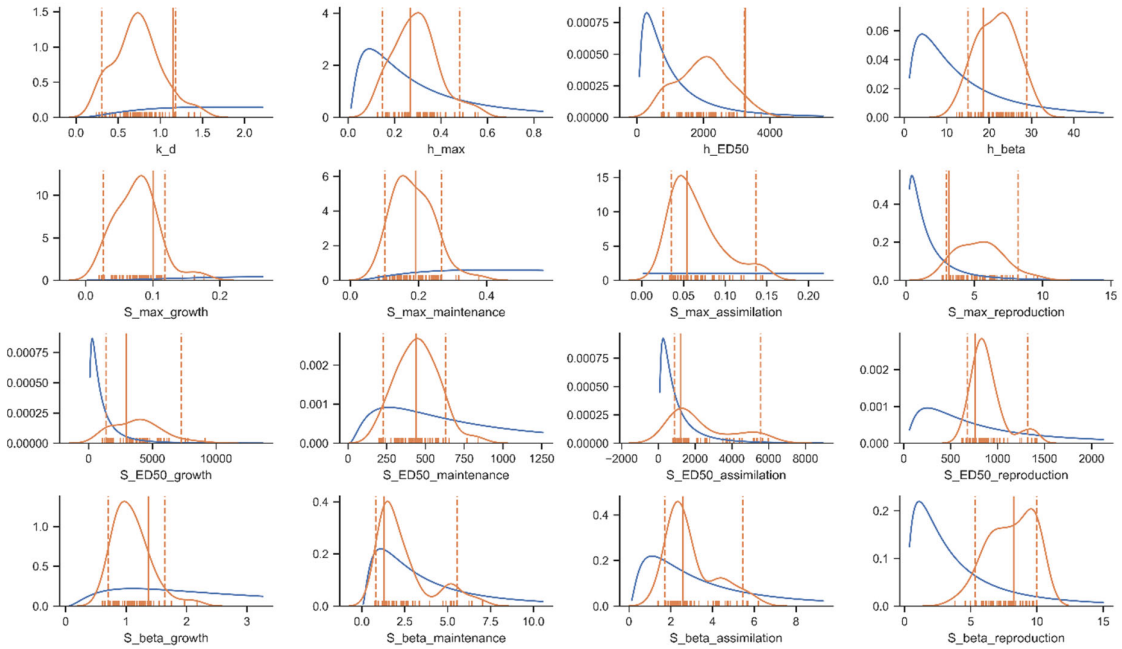

SI Figure 6 Prior (blue) and posterior (orange) probability density of TKTD parameters for Nickel. Vertical bars indicate marginal 90% credible intervals. Point estimates can differ from the value associated with the highest probability density due to covariance.

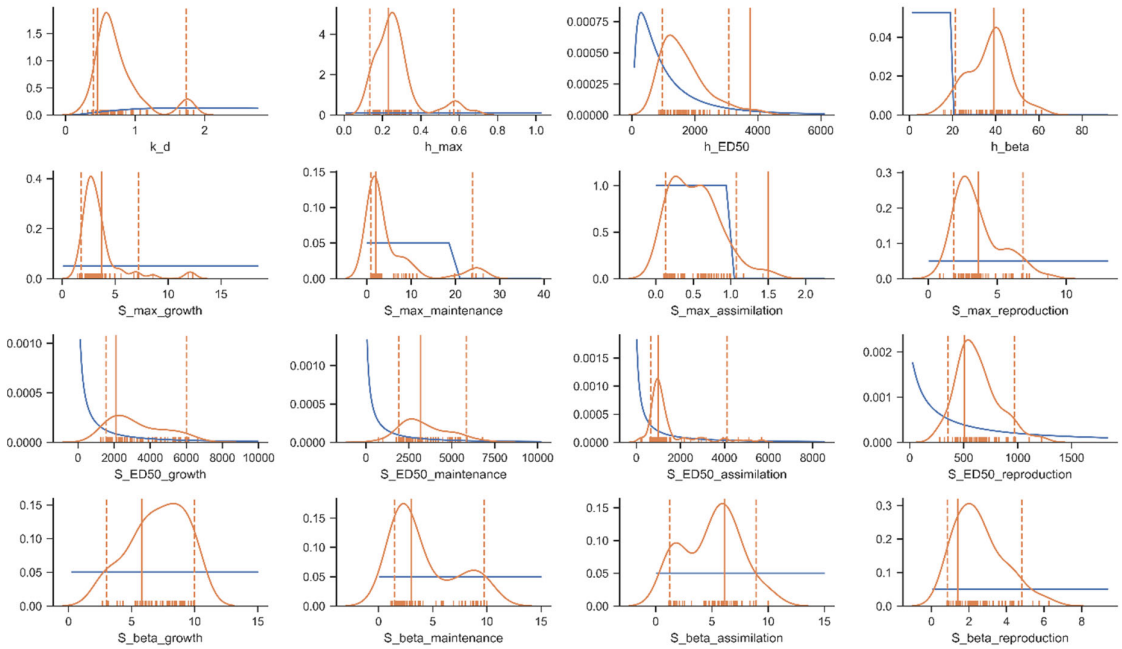

SI Figure 7 Prior (blue) and posterior (orange) probability density of TKTD parameters for Zinc. Vertical bars indicate marginal 90% credible intervals. Point estimates can differ from the value associated with the highest probability density due to covariance.

SI Table 6 Point estimates and marginal credible intervals of TKTD parameters for Copper. PMoAs are indicated by subscripts; G=increase in growth costs, M=increase in somatic and maturity maintenance costs, A=decrease in assimilation flux, R=decrease in reproduction efficiency. Subscript h denotes that a parameter is linked to hazard rate (direct lethal effects); subscript S denotes that a parameter is linked to stress (sublethal effects via PMoA).

parameter (unit)	**estimate**	**CL5**	**CL95**
$k_{d,Cu}$ (day^{-1})	0.63	0.61	1.7
$h_{max,Cu}$ (day^{-1})	0.56	0.52	2.6
$ED50_{h,Cu}$ (nM)	8.6	5.5	12
$\beta_{h,Cu}$ (-)	18	8.3	28
$S_{max,Cu,G}$ (-)	3.1	1.2	4.5
$S_{max,Cu,M}$ (-)	0.52	0.4	1.4
$S_{max,Cu,A}$ (-)	0.043	0.057	0.16
$S_{max,Cu,R}$ (-)	1.7	0.95	2.3
$ED50_{S,Cu,G}$ (nM)	4.1	4.4	28
$ED50_{S,Cu,M}$(nM)	37	9.7	41
$ED50_{S,Cu,A}$ (nM)	18	6.3	39
$ED50_{S,Cu,R}$ (nM)	0.73	0.75	3
$\beta_{S,Cu,G}$ (-)	6.3	2.1	9
$\beta_{S,Cu,M}$ (-)	1.5	1	6.2
$\beta_{S,Cu,A}$ (-)	10	3.2	10
$\beta_{S,Cu,R}$ (-)	1.9	0.78	2.6

SI Table 7 Point estimates and marginal credible intervals of TKTD parameters for Nickel. PMoAs are indicated by subscripts; G=increase in growth costs, M=increase in somatic and maturity maintenance costs, A=decrease in assimilation flux, R=decrease in reproduction efficiency. Subscript h denotes that a parameter is linked to hazard rate (direct lethal effects); subscript S denotes that a parameter is linked to stress (sublethal effects via PMoA).

parameter (unit)	**estimate**	**CL5**	**CL95**
$k_{d,Ni}$ (day^{-1})	1.2	0.31	1.2
$h_{max,Ni}$ (day^{-1})	0.27	0.15	0.48
$ED50_{h,Ni}$ (nM)	3300	780	3200
$\beta_{h,Ni}$ (-)	19	15	29
$S_{max,Ni,G}$ (-)	0.1	0.026	0.12

$S_{max,Ni,M}$ (-)	0.19	0.1	0.27
$S_{max,Ni,A}$ (-)	0.054	0.035	0.14
$S_{max,Ni,R}$ (-)	3.1	3	8.2
$ED50_{S,Ni,G}$ (nM)	2900	1400	7300
$ED50_{S,Ni,M}$(nM)	440	230	630
$ED50_{S,Ni,A}$ (nM)	1200	870	5600
$ED50_{S,Ni,R}$ (nM)	760	680	1300
$\beta_{S,Ni,G}$ (-)	1.4	0.71	1.6
$\beta_{S,Ni,M}$ (-)	1.3	0.82	5.6
$\beta_{S,Ni,A}$ (-)	2.6	1.7	5.4
$\beta_{S,Ni,R}$ (-)	8.3	5.3	10

SI Table 8 Point estimates and marginal credible intervals of TKTD parameters for Zinc. PMoAs are indicated by subscripts; G=increase in growth costs, M=increase in somatic and maturity maintenance costs, A=decrease in assimilation flux, R=decrease in reproduction efficiency. Subscript h denotes that a parameter is linked to hazard rate (direct lethal effects); subscript S denotes that a parameter is linked to stress (sublethal effects via PMoA).

parameter (unit)	**estimate**	**CL5**	**CL95**
$k_{d,Zn}$ (day^{-1})	0.46	0.41	1.7
$h_{max,Zn}$ (day^{-1})	0.23	0.13	0.57
$ED50_{h,Zn}$ (nM)	3800	970	3100
$\beta_{h,Ni}$ (-)	39	21	53
$S_{max,Zn,G}$ (-)	3.7	1.8	7.2
$S_{max,Zn,M}$ (-)	2	0.95	24
$S_{max,Zn,A}$ (-)	1.5	0.13	1.1
$S_{max,Zn,R}$ (-)	3.6	1.8	6.9
$ED50_{S,Zn,G}$ (nM)	2100	1600	6000
$ED50_{S,Zn,M}$(nM)	3200	1900	5900
$ED50_{S,Zn,A}$ (nM)	1000	660	4100
$ED50_{S,Zn,R}$ (nM)	510	350	970
$\beta_{S,Zn,G}$ (-)	5.8	3	10
$\beta_{S,Zn,M}$ (-)	3	1.5	9.7

$\beta_{S,Zn,A}$ (-)	6.1	1.3	9
$\beta_{S,Zn,R}$ (-)	1.4	0.87	4.8

Monte-Carlo simulations for identification of dominant pMoAs

Metals were allowed to act via multiple pMoAs simultaneously. Solely by inspecting TKTD parameters, it is difficult to make a reliable statement about which pMoAs were driving toxicity in the DEB-IBM simulations, because their relative importance is steered by multiple parameters simultaneously. We therefore conducted additional Monte-Carlo (MC) simulations, allowing to evaluate visually which pMoAs explained most of the effects predicted by the full model. The MC simulation scheme proceeded as follows:

1. Sample a particle θ_{DEB} from the joint posterior distribution of DEB parameters, and a particle $\theta_{TKTD,i}$ from the joint posterior distribution of TKTD parameters of metal i.
2. For a given $\theta_{DEB}/\theta_{TKTD}$-combination, iterate over toxicity components (lethal effects or one of the four pMoAs) :
    1. Within θ_{TKTD}, set all $S_{max,i,j}$ values and $h_{max,i}$ to 0, expect for the parameter linked to the current toxicity component ($h_{max,i}$ for lethal effects or $S_{max,i,j}$ for pMoA j). This yields a model where only one toxicity component is active.
    2. Simulate the single-metal toxicity test with θ_{DEB} and the modified θ_{TKTD} as input.
3. Simulate the single-metal toxicity test with the originally samples $\theta_{DEB}/\theta_{TKTD}$-combination.
4. Repeat steps 1-3 100 times.

The result of this scheme is a time-series of relative responses of population density over time, split up by toxicity component and with an associated uncertainty. The MC scheme was conducted separately for each metal.

Predicted individual-level state variables

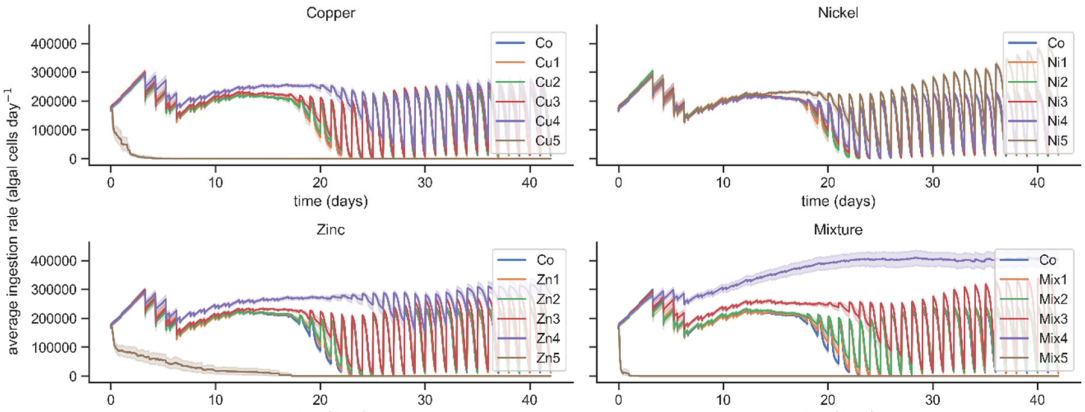

SI Figure 8 Average food ingestion rates over time per metal treatment in the simulations. Shaded areas show 90% confidence intervals of average ingestion rates (result of simulating 100 posterior samples).

In the following, we provide some more detailed information on individual-level state variables that were predicted by the DEB-IBM.

Predicted patterns of feeding and assimilation in the DEB-IBM

Average food ingestion rates followed a distinct pattern, where after some time during the simulation (typically coinciding with peak densities), ingestion rates strongly oscillated on a daily basis. Quickly oscillating ingestion rates emerged as a result of daily addition of food, which is entirely consumed at high population densities. The onset of this oscillating pattern therefore also indicates the onset of (strong) food competition. In each case, the onset of food competition was delayed in time as a function of increasing metal exposure, and average ingestion rates are increased during the phase of competition (more so for Ni and Zn than for Cu). In the mixture, this effect was larger than in the single-metal treatments (SI Figure 8). Since ingestion rates are size-specific, one might argue that this is simply a result of changes in population structure. We can state that this is not the case, because the same pattern is found for the scaled functional response (i.e., ingestion rate relative to the maximum surface area-specific ingestion rate), which only depends on the half-saturation constant for food uptake and the current food density, and not on size.

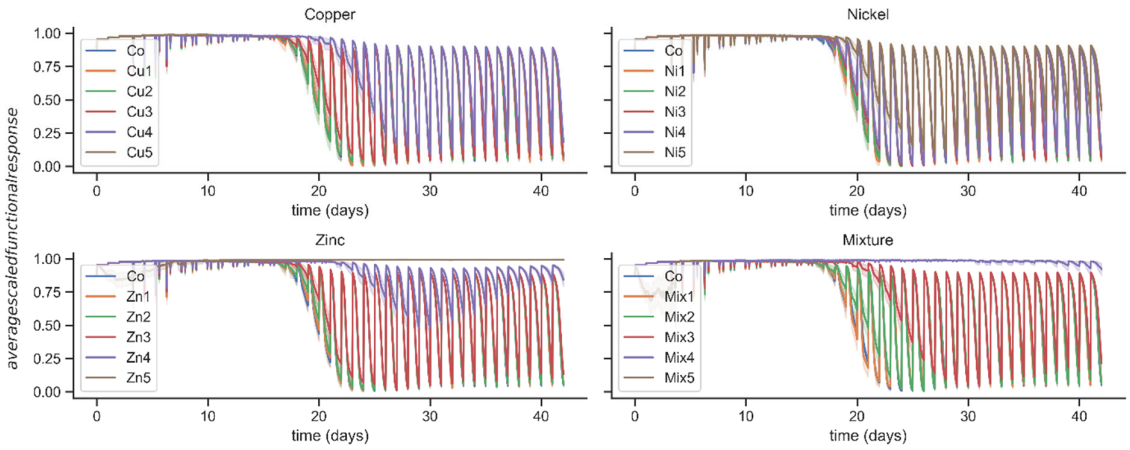

211

212 *SI Figure 9 Average scaled functional responses over time per metal treatment in the simulations. Shaded areas show 90%*
213 *confidence intervals of average ingestion rates (result of simulating 100 posterior samples).*

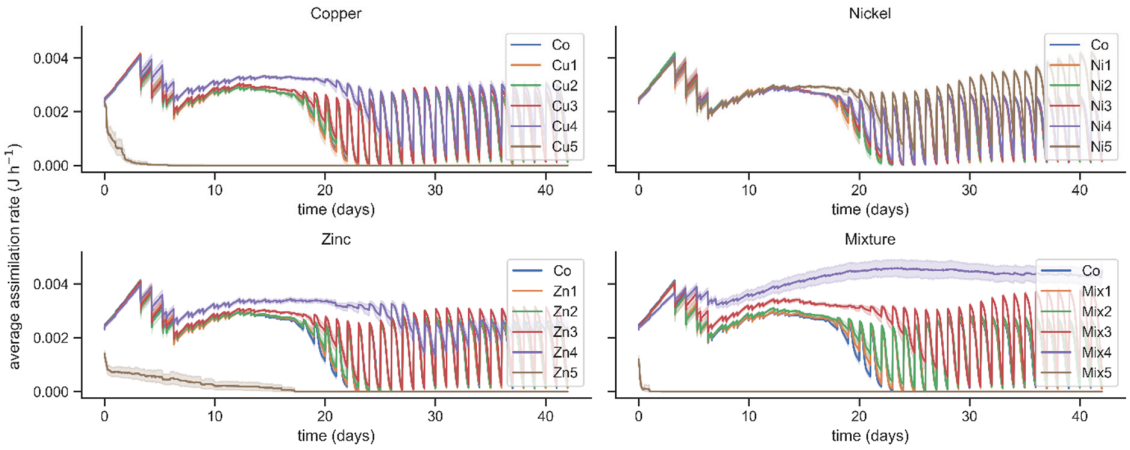

214

215 *SI Figure 10 Average assimilation rates over time per metal treatment in the simulations. Shaded areas show 90%*
216 *confidence intervals of average ingestion rates (result of simulating 100 posterior samples).*

217 For Cu and Ni, trends in assimilation rates were qualitatively identical with trends in
218 ingestion rates. In the case of Zn, direct effects on assimilation rate via the corresponding
219 pMoA mitigated the stimulation of assimilation rate at higher Zn concentrations (towards
220 equilibrium, ingestion rates in treatment Zn3 were lower than in Zn4. For assimilation rates,
221 the trend was reversed, SI Figure 10). Importantly, the stimulation of assimilation rates in
222 the mixtures was again comparable to the stimulation of ingestion rates in the mixtures. This
223 suggests a mechanism that explains antagonistic effects of the mixture: Part of the effects of
224 Zn on assimilation rate were ameliorated by population-level processes (release from
225 competition, increased average energy assimilation), which were induced by exposure to Cu

226 and Ni. The antagonistic effects on growth rate and 6-week density can thus be seen as a
227 result of the interplay between pMoAs reproduction efficiency and assimilation rate.

Metal Mixture Toxicity To *Daphnia Magna* Populations: ODD Model Description[1]

[1]The model description follows the ODD (Overview, Design concepts, Details) protocol for describing individual- and agent-based models (Grimm et al. 2006, 2010[2]).

1. Purpose

The purpose of the model is to predict mixture toxicity of ionic Copper (Cu), Nickel (Ni) and Zinc (Zn) to *Daphnia magna* populations in semi-static 42-day microcosm tests.

2. Entities, state variables, and scales

Fleas

The central entity of the IBM implementation are *D. magna* individuals. In the Julia code, they are implemented as a composite type called *Flea.* Each *Flea* has the following primary attributes (parameters).

[1] References are given in the manuscript.

Symbol	Julia identifier	Julia data type	unit	description
-	unique_id	Int64	-	Identifying number
K	K	Float64	(# cells L^{-1})	Half-saturation for food uptake
$\{\dot{J_{X,m}}\}$	J_X_Am_rate	Float64	(# cells cm^{-2} day^{-1})	Maximum surface area-specific ingestion rate
$U_{H,b}$	U_Hb	Float64	cm^2	Scaled maturity at birth
$U_{H,p}$	U_Hp	Float64	cm^2	Scaled maturity at puberty
$\dot{k_M}$	k_M_rate	Float64	day^{-1}	Somatic maintenance rate constant
$\dot{k_J}$	k_J_rate	Float64	day^{-1}	Maturity maintenance rate constant
g	g	Float64	-	Energy investment ratio
$\dot{v}$	v_rate	Float64	cm day^{-1}	Conductance rate
κ	kap	Float64	-	Somatic investment ratio

κ_R	kap_R	Float64	-	Reproduction efficiency
d_M	shape_factor	Float64	-	Conversion from structural length to carapace length
m_e	mortality_constant	Float64	-	starvation mortality
s_G	sG	Float64	-	Gompertz stress coefficient
h_A	h_a	Float64	day^{-2}	Weibull ageing acceleration
τ_{molt}	time_between_molts	Float64	days	molting intervals
$k_{d,i}$	k_d	Array{Float64,1}	day^{-1}	dominant rate constant (1d Array, one value per metal)
$S_{max,i,j}$	S_max	Array{Float64,2}	-	Maximum physiological stress
$ED50_{i,j}$	S_ED50	Array{Float64,2}	nM Me^{2+}	Median effective damage
$\beta_{i,j}$	S_beta	Array{Float64,2}	-	Hill's slope for sublethal effects
$h_{max,i}$	h_max	Array{Float64,1}	day^{-1}	Maximum hazard rate

$ED50_{h,i}$	h_ED50	Array{Float64,1}	nM Me^{2+}	Median effective damage for lethal effects
$\beta_{h,i}$	h_beta	Array{Float64,1}	-	Hill's slope for lethal effects
–	scatter_multiplier	Float64	-	Random factor for individual variability

Subscript i refers to metal i and subscripts j refers to metal j. One-dimensional arrays contain one value for every metal, two-dimensional arrays contain one value for every metal and physiological Mode of Action (pMoA).

The state variables that fully describe a *Flea*'s state are as follows:

Symbol	**Julia identifier**	**Julia data type**	**unit**	**description**
U_E	U_E	Float64	cm^2	scaled reserves
U_H	U_H	Float64	cm^2	scaled maturity
U_R	U_R	Float64	cm^2	scaled reproduction buffer
$\dot{h_a}$	h_rate	Float64	day^{-1}	ageing hazard rate
$\ddot{q}$	q_acceleration	Float64	day^{-2}	ageing acceleration
L	L	Float64	cm	structural length
f	f	Float64	-	scaled functional response

S_A	S_A	Float64	cm^2	scaled assimilation flux
S_C	S_C	Float64	cm^2	scaled mobilization flux
e	e_scaled	Float64	-	scaled reserve density

The DEB-IBM implementation is based on the scaled DEB model, where assimilation rate is scaled out of the model. Not the primary parameters are used directly in the model, but the compound parameters which depend on primary parameters.

The maximum surface-area specific ingestion rate $J_{X,A,m}$ depends on maximum assimilation rate and assimilation efficiency, following from the basic principle that assimilation rate is the product of ingestion rate and assimilation efficiency.

$$J_{X,A,m} = \frac{p_{A,m}}{\kappa_{E,X}}$$

Because food density is expressed in algal cell density, not energy, a conversion from algal cells to energy is implied in the assimilation efficiency $\kappa_{E,X}$.

The parameter K (algal cells L^{-1}) is the half-saturation constant for food uptake. In the context of DEB theory, it is a compound parameter and therefore calculated from primary parameters:

$$K = \frac{J_{X,A,m}}{F_m}$$

Environment

The simulated environment is fully described by the current food density X_t (cells L^{-1}) and the vector of current metal free ion activities C_t (nM). The temporal resolution TR is set to 24 time-steps per day, so that one model time-step corresponds to one hour.

3. Process overview and scheduling

A single model step proceeds as follows:

1. Randomize order of individuals
2. For every individual
    a. Toxicity submodel
        i. Determine death due to direct lethal effects
        ii. Calculate and apply sublethal metal stress
    b. Feeding submodel
        i. Calculate ingestion rates

ii. Update environmental food density

c. Calculate change in scaled DEB state variables $\frac{dU_E}{dt}$, $\frac{dU_H}{dt}$, $\frac{dU_R}{dt}$, $\frac{dL}{dt}$

d. Ageing submodel ($\frac{d\ddot{q}}{dt}$, $\frac{dh_a}{dt}$)

e. Update state variables

f. Reproduction submodel

i. Determine number of offspring released

ii. Initialize embryos as new Fleas

g. Starvation submodel

h. Mortality submodel

3. Update environment

i. Add food once per day

ii. Remove a fraction of food equal to the fraction of medium renewed.

4. Remove individuals which have been determined to die

4. Design concepts

Emergence. Effects of metal mixtures on individual life-history and population dynamics emerge from interactions via metabolic pathways. Population density emerges from individual state-variables and resource limitation

Stochasticity. The following processes are stochastic:

- Individual variability introduced via scatter multiplier applied to $p_{A,m}$.
- Death due to starvation, lethal metal effects or ageing.
- Food addition. A random factor is applied to the amount of food added daily, to account for slight variations in the exact amount of algal cells that is added to the medium.

Observation. The total number of individuals is recorded at the end of every time-step, as well as population-averages of selected state variables (ingestion rate, scaled functional response, scaled assimilation flux).

5. Initialization

At t=0, a fixed number of 2 adult and 10 juvenile Fleas are initialized. For juveniles, a random age between 0 and 24 hours is sampled and their life-history up to the random age is simulated. This is done given *ad libitum* feeding conditions (f=1). The same is done for initial adults, which are old enough so that $U_H \geq U_{H,p}$, but not more than 21 days old.

6. Input data

To simulate metal toxicity tests, a CSV file containing metal free ion activities for every metal at every time-step is needed.

Remaining global input parameters that have to be given to run a simulation are the maximum simulated time t_{max} (days), the amount of food added daily (# algal cells), the intervals at which medium renewals are simulated and the fraction of medium renewed.

7. Submodels

Toxicity

Following GUTS-RED, external concentrations $C_{W,i}$ (nM Me^{2+}) of metal i were directly translated to scaled damage $D_{W,i}$, (nM Me^{2+}) controlled by a single parameter, the dominant rate constant k_d (day^{-1}):

$$\frac{dD_{W,i}}{dt} = k_{d,i} \times (C_{W,i} - D_{W,i})$$

Sublethal and lethal effects were modelled as a function of a common damage pool $D_{W,i}$ for each metal.

In the case of lethal effects, we related $D_{W,i}$ to a hazard rate $h_{z,i}$ (day^{-1}) using a log-logistic equation, and converted $h_{z,i}$ to a stochastic mortality probability $p_{z,i}$.

$$h_{z,i} = \frac{h_{max,i}}{1 + \left(\frac{D_{W,i}}{ED50_{h,i}}\right)^{-\beta_{h,i}}}$$

$$p_{z,i} = \mathrm{e}^{-\mathrm{h_{z,i}}}$$

We thus assumed a stochastic death mechanism. $p_{z,i}$ was evaluated independently for each metal. $ED50_{h,i}$ (nM) is the scaled internal damage that leads to 50% of the maximum hazard rate caused by stressor i, $h_{max,i}$; $\beta_{h,i}$is the corresponding Hill's slope.

For implementation of sublethal effects, we related $D_{W,i}$ to physiological stress S_i specific for pMoA j:

$$S_{i,j} = \frac{S_{max,i,j}}{1 + \left(\frac{D_{W,i}}{ED50_{S,i,j}}\right)^{-\beta_{S,i,j}}}$$

$ED50_{S,i,j}$ is the 50% effective damage of metal i with respect to pMoA j. $S_{max,i,j}$ $(-)$ is the corresponding maximum stress level. The state variable $S_{i,j}$ modifies physiological processes based on the physiological Mode of Action (pMoA). We considered the four most commonly considered pMoAs, being 1), increase in growth costs, 2) increase in somatic and maturity maintenance costs, 3) decrease in assimilation flux, 4) decrease in reproduction efficiency.

pMoA	**stressed value**
Increase in growth costs (G)	$g \rightarrow g(1 + S_{i,G})$
	$\dot{k}_M \rightarrow \dot{k}_M \frac{1}{1 + S_{i,G}}$
Increase in maintenance costs (M)	$\dot{k}_M \rightarrow \dot{k}_M(1 + S_{i,M})$
	$\dot{k}_J \rightarrow \dot{k}_J(1 + S_{i,M})$
Decrease in assimilation flux (A)	$S_A \rightarrow S_A(1 - S_{i,A})$

Decrease in reproduction efficiency (R)	$\kappa_R \rightarrow \kappa_R(\frac{1}{1+S_{i,R}})$

For mixtures of metals acting via shared pMoAs, effects of multiple metals via the same pMoA are combined by multiplying the individual effects, so $g \rightarrow g\prod_{i=1}^{n}(1+S_{i,G})$, $\dot{k}_M \rightarrow \dot{k}_M\prod_{i=1}^{n}(1+S_{i,M})$, etc.

Feeding And Assimilation

A Type II functional response was implemented to describe dependency of ingestion and assimilation rate on environmental food density. The corresponding state variable is the scaled functional response f, which is calculated from food density X (algal cells L^{-1}).

$$f = \frac{X}{X+K}$$

The combination of f, $J_{X,A,m}$ and an individual's squared structure length L (cm) gives us its ingestion rate:

$$\dot{J_X} = fJ_{X,A,m}L^2$$

The scaled assimilation flux S_A (cm^2) depends only on f, L^2 and the combined metal effects, because assimilation rate is scaled out of the model.

$$S_A = fL^2\prod_{i=1}^{n}1-S_{i,A}$$

S_A has the perhaps counter-intuitive dimension "area". If an estimate of $p_{A,m}$ is available, S_A can be converted to actual assimilation rate $\dot{p}$ (J day^{-1}) by multiplying with $p_{A,m}$. This was done for visualization purposes.

Change in SCALED DEB parameters

The change in scaled DEB parameters is calculated as specified in the scaled DEB model.

Change in scaled reserves $\frac{dU_E}{dt}$ is the difference between scaled assimilation and mobilization fluxes, S_A and S_C (see "feeding and assimilation" for definition of S_A).

$$S_C = L^2\left(\frac{ge}{g+e}\right)\left[1+\left(\frac{L}{g\left(\frac{\dot{v}}{g\,\dot{k}_M}\right)}\right)\right]$$

$$\frac{dU_E}{dt} = S_A - S_C$$

Given below are the difference equations for the remaining scaled DEB state variables.

$$\frac{dU_H}{dt} = \begin{cases}(1-\kappa)S_C - \dot{k}_J U_H \; if \; U_H < U_{H,p} \\ 0 \; otherwise\end{cases}$$

$$dU_R = \begin{cases}0 \; if \; U_H \le U_{H,p} \\ (1-\kappa)S_C - \dot{k}_J U_H \; otherwise\end{cases}$$

$$dL = \frac{1}{3}\frac{\dot{v}}{gL^2}S_C - \dot{k}_M L$$

Starvation

A starvation-induced mortality probability p_e is calculated. It increases linearly with decreasing reserve density.

$$p_e = (1-e)(m_e)^{\frac{1}{TR}}$$

The temporal resolution TR (timesteps day^{-1}) corrects for the temporal resolution at which the IBM is executed (24 timesteps day^{-1} by default).

Reproduction

While the reproduction buffer U_R is updated at every model time-step, reproduction itself is implemented as a continuous process. Reproduction occurs during molting, controlled by the molting period τ_{molt} (days), which is constant for an individual, but subject to individual variability.

If the time since the last molting event is larger or equal to τ_{molt}, reproduction is triggered.

The number of offspring produced n_{eggs} is

$$n_{eggs} = \left\lfloor \frac{U_R \kappa_R}{U_{egg}} \right\rfloor$$

$\lfloor x \rfloor$ denotes the floor function. The reproduction efficiency κ_R controls which fraction of the energy allocated to reproduction is effectively converted to embryonal reserve. U_{egg} (t cm^2) is the energy investment per egg. It is not an independent parameter, but internally derived from primary parameters numerically, using a bisection method.

The reproduction buffer is immediately updated, implying that $1 - \kappa_R$ of the invested reproduction buffer is lost in the process.

$$U_R = U_R - \left\lfloor \frac{U_R}{U_{egg}} \right\rfloor U_{egg}$$

The appropriate number of juveniles is initialized. Individual variability is applied to the new individuals and they are added to the population.

Ageing

The process of ageing is controlled by the ageing acceleration $\ddot{q}$. On a conceptual level, this represents an accumulation of damage over time, which is self-amplifying.

$$\frac{d\ddot{q}}{dt} = \left\{ \ddot{q} \left[\frac{L^3}{\left(\frac{\dot{v}}{g \dot{k}_M} \right)^3} \right] s_G h_a \right\} \left\{ e \left[\frac{\dot{v}}{L} - \left(\frac{3}{L} \frac{dL}{dt} \right) \right] - \left(\frac{3}{L} \frac{dL}{dt} \ddot{q} \right) \right\}$$

Ageing acceleration is linked to an ageing-related hazard rate $\dot{h}_a$.

$$\frac{d\dot{h}_a}{dt} = \ddot{q} - \left(\frac{3}{L} dL\right) \dot{h}_a$$

Mortality

Mortality is implemented as a stochastic process. The mortality probabilities resulting from each possible cause of death (ageing, starvation, metal toxicity) are applied independently. Death occurs if at least one of the following conditions holds true, where u_i is a random number sampled from the uniform distribution $U(0,1)$.

$$u_1 < (1 - e)(m_e)^{\frac{1}{TR}}$$

$$u_2 < 1 - \left(\dot{h}_a\right)^{\frac{1}{TR}}$$

$$u_3 > \exp\left(-\frac{h_{Cu}}{TR}\right)$$

$$u_4 > \exp\left(-\frac{h_{Ni}}{TR}\right)$$

$$u_5 > \exp\left(-\frac{h_{Zn}}{TR}\right)$$